Università degli Studi di Padova
Department of Mathematics "Tullio Levi-Civita"
Master Degree in Data Science

Reliable IEEE 802.15.4g-based Smart Utility Networks via Adaptive Modulation Selection and Re-Transmission Shaping

Supervisor: Prof. Michele Rossi
Department of Information Engineering, Università Degli Studi di Padova

Co-Supervisor: Dr. Pere Tuset-Peiró
Computer Science, Multimedia and Telecommunications Department, Universitat Oberta de Catalunya

Intership Supervisor: Prof. Xavier Vilajosana
Department IN3, Universitat Oberta de Catalunya

Student: Domenico Solimini
N. 1206034

Academic Year 2019-2020

Abstract

In this thesis work we propose and evaluate a strategy to improve transmission in IEEE 802.15.4g SUN networks. This kind of network is at the basis of many promising IoT applications that require a high reliability while maintaining low power consumption.

The proposed strategy consists in two distinct parts: re-transmission shaping and modulation selection. The re-transmission shaping mechanism keeps track of unused packet re-transmissions and allocates additional re-transmissions when the instantaneous link quality decreases due to channel impairments. The modulation selection strategies apply Multi Armed Bandits algorithms to dynamically choose the best transmission modulation. The combined effect of these two mechanisms aims to maximize link reliability, while minimizing energy consumption and meeting radio-frequency regulation constraints.

To evaluate the proposed methods we use trace-based simulations using a IEEE 802.15.4g SUN data-set and two widely used metrics, the PDR (Packet Delivery Ratio) and the RNP (Required Number of Packets).

The obtained results show that re-transmission shaping and modulation selection are useful mechanism to improve link reliability of low-power wireless communications. Their combined use can increase PDR from 77.9% to 98.7% while sustaining a RNP of 1.7 re-transmissions per packet, when compared to using a single re-transmission per packet.

Contents

Preface

The pervasive adoption of wireless communications is at the basis of new industrial and social paradigms that are likely to deeply impact on both economy and personal life. The possibility of allowing objects of everyday life with micro-controllers and radio transceivers for digital communication opens up a new world of potential services.

The *Internet of Things* (IoT) is a recent paradigm in which the objects of everyday life will be able to communicate between them and with the users, becoming an integral part of the Internet. Heterogeneous end devices communicate without human intervention, a kind of communication known as machine-to-machine (M2M) communication. A big challenge for the actual realization of the IoT paradigm is the creation of a environment able to integrate a wide variety of smart devices provided with different communication stacks.

There is a variety of application domains that will be impacted by IoT: in [Gubbi et al., 2013] it is presented a list of distinction between personal and home, enterprise, utilities, and mobile domains, depending on the scale interested by the network.

Within the variety of application of IoT, *Smart City* is worthy of specific attention, due to the huge social impact that it is likely to have. Smart City is a model that aims at exploiting the most advanced communication technologies to support added-value services for the administration of the city and for the citizens. It relies on a wide IoT architecture, spread across a whole city interconnecting public buildings and infrastructures, means of transport, and public services providers. It should be also able to interconnect with private citizens and to integrate with existing communication infrastructures to support a progressive evolution and re-shaping of the IoT by connecting new devices and deploying new functionalities and services. The effects of this urban architectural model are not restricted to the increased efficiency in service provision but can also promote the awareness and the active participation of citizens in public matters [A. Mulligan and Olsson, 2013].

Among the services that can be offered in such an autonomous and interconnected fashion, it can be mentioned building structural health, air quality monitoring,

noise monitoring, traffic congestion, city energy consumption, smart parking, smart lighting, and automation and salubrity of public buildings. All these services may rely on wireless network based on the IEEE 802.15.4 standard, with traffic rates around 1 packet every 10 minutes per device [Zanella et al., 2014]. Depending on the application these services may be battery operated or rely on energy harvesting, i.e. based on devices capable of retrieving small amount of energy from ambient background. In both cases it is evident how the energetic efficiency of the end devices, in addition to an efficient data delivery, is of substantial importance to allow the effective deployment of these services.

A relevant example of successfully experimental implementation of a Smart City infrastructure is "Padova Smart City" project [Castellani et al., 2011]. It consists in a network of wireless sensors presenting more than 300 nodes deployed at the University of Padova. Its aim is to promote the adoption of open data and advanced telecommunication solutions in the public administration. The network consists in nodes equipped with different kinds of sensors, placed on street light poles. The nodes control the public street lighting in an efficient way by measuring the light intensity at each post, and collect environmental data such as CO level, air temperature and humidity, vibrations, noise, and so on.

This example, as many others exciting applications, relies on the possibility of providing a reliable communication infrastructure, able to meet the energy requirements of low-power end devices. The IEEE 802.15.4 standard is a promising technology in this direction. This work analyzes a specific use-case in which a IEEE 802.15.4 SUN network is deployed in a challenging environment. The proposed solutions increase the network reliability while meeting low power consumption requirements.

Chapter 1

Introduction

1.1 Problem overview

In this work we propose and discuss two mechanisms to enhance reliability in a IEEE 802.15.4g-based wireless network. The network used to evaluate the mechanisms presents some specific characteristics; in spite of this, the methods have not been designed specifically for the network in use and the analysis provided in this work are expected to provide general results.

The network used to provide data to validate the methods has been installed in a warehouse located in Madrid for industrial purposes. It is composed by 11 sensors and one central gateway that collects the environmental variables sensed by the end-nodes (like humidity, pressure, temperature etc.). A general requirement for this kind of network is the ease of installation and maintenance. Therefore any kind of wired connections should be avoided and the battery of the devices should last for a long time.

The presence of sophisticated tools to improve the packet delivery strategies (like channel synchronization between sensor and gateway) is not compatible with these simplicity requirements. The sensor nodes are supposed to have a limited computing power, both to reduce the battery drain and to keep the sensor hardware cheap and simple.

The objective of this work is to provide a transmission mechanism able to reach 99% of successfully transmitted packets while keeping the battery drain under a threshold that should be set in each specific implementation. It is important, once specified the threshold, not to overcome this value. Any solution consistent with the power efficiency requirements and able to provide the required PDR value, however, is to be considered as equally good. This is justified by reasons of practical utility: the

batteries of the sensors should be re-charged regularly (e.g. every 2 years), when the time expires the batteries are re-charged and the presence of eventual residual power becomes irrelevant. In a more general scenario, even considering energy harvesting devices, it is reasonable to consider an average energy consumption that should not be exceeded. For example a solar-powered device is re-charged every day when it is exposed to the sun light and the energy consumption rate shouldn't be allowed to overcome the average energy provided daily by the solar cell. Under this consumption rate, any energetic behaviour is fine.

The environment in which the network has been deployed constitutes an additional challenge to the network reliability. As in many indoor scenarios, the problems of signal attenuation and multi-path propagation compromise the quality of the signal. In an industrial scenario (like the one in which the analyzed network has been deployed), these problems show up with even more intensity, due to the abundance of reflective metal surfaces. In addition, the presence of other wireless networks that may operate in the same frequency band increases the environment problematic.

The second main challenge posed by this kind of setting is due to the non-stationary nature of the environment. Machinery are allowed to move into the warehouse, modifying the multi-path propagation of the signal, and scaffolds may be filled or cleaned out, thus shielding or allowing the direct propagation of the signal between two nodes. This leads to the necessity of developing algorithms able to handle the non-stationarity of the environment.

1.2 Original Contribution

In this work we propose two mechanisms to enhance the channel reliability in IEEE 802.15.4g networks as alternative to the established methods.

Packet re-transmissions is the most straightforward way to guarantee data delivery over unreliable wireless links. It simply consists in re-transmitting each data packet up to n times until an acknowledgement packet is received successfully. If the acknowledgement is not received within n repetitions and the transmission process expires, the data packet is considered lost. Even though effective, this approach poses various problems, the most important of which is the high energy expenditure that might be required. In addition to that, it is possible to observe a channel correlation, i.e. multiple consecutive re-transmissions are likely to present the same outcome, thus reducing the usefulness of re-transmitting a lost packet over the same channel.

Hence, the proposed methods have been designed to overcome these limitations, enabling a more robust and energy-efficient signal transmission. These methods are:

- **Modulation selection**: dynamic choice of the best modulation for each packet re-transmission depending on channel condition based on Multi Armed Bandit algorithms;

- **Re-transmission shaping**: better redistribution of available packet re-transmissions while meeting energy constraints.

Re-transmission shaping has been presented in 17th ACM Symposium on Performance Evaluation of Wireless Ad Hoc, Sensor, & Ubiquitous Networks (PE-WASUN'20) [Solimini et al., 2020]. Multi armed bandit algorithms have already been applied in wireless network field for modulation selection, but not in the same context. This method and its combined effect with re-transmission shaping will be soon presented in [Solimini et al., 2021]. In this thesis work are present contributions from both the articles, together with further explanations and a more detailed presentation of the background and the evaluation process.

1.3 Organization

This thesis is organized in this first introductory part plus five other chapters and a conclusion.

Firstly, Chapter 2 describes the general behaviour of a wireless channel with specific emphasis to the signal deterioration due to multi path propagation and interference. These effects are particularly relevant in the dataset analyzed in this work.

Chapter 3 presents the related work, firstly describing in detail the IEEE 802.15.4g standard with its associated SUN modulations (i.e., SUN-FSK, SUN-OQPSK and SUN-OFDM) in Section 3.1. Then Section 3.2 discusses the efforts made to guarantee the reliability of a IEEE 802.15.4g network and, finally, Section 3.3 presents some relevant case of application of Multi Armed Bandits to the channel selection problem in wireless networks.

This studies are interesting to introduce the modulation selection strategies described in Chapter 4. This chapter presents the two methods introduced in this work to increase the network reliability i.e. the re-transmission shaping mechanism in Section 4.1 and the modulation selection strategies in Section 4.2 with a description of the combined methods in Section 4.3.

Chapter 5 discusses the evaluation methodology consisting in the data acquisition part comprehensive of a first data pre-processing (in Section 5.1 and in the simulation of the packets transmission within the network by applying the proposed methods

separately and in conjunction. Within this Chapter, Section 5.2.1 presents the parameters used to evaluate the network performances in this work, namely the Packet Delivery Ratio (PDR) that indicates the ratio of successfully transmitted packets over the total number of transmission attempts, and the required Number of Packet Transmissions (NRP), used to take trace of the average number of re-transmissions needed to send a packet. Section 5.2.2 presents the modulation selection strategies used to compare the results obtained with the proposed methods.

The experimental results are presented in Chapter 6, separately for the re-transmission shaping and modulation selection, and then jointly. It is shown how the combined effect of the two proposed mechanisms is capable of reaching the target transmission efficiency of 99% while meeting the energy constraints.

Finally, Chapter 7 draws the conclusions of the whole work, describing also some possible further developments that can be explored to extend and improve the results obtained in this work in Section 7.2.

Chapter 2

Wireless Communications Background

This Chapter provides the background to understand the problems posed by a pervasive application of wireless communication devices in urban and industrial environments like the one in which the network analyzed in this work has been deployed. Sections 2.1 and 2.2 contain respectively a general description of the properties of the transmission of an electromagnetic wave-front in a complex environment, and a description of the interference phenomena that a wireless device operating in an unlicensed band could face.

2.1 Signal Propagation

Wireless communications pose several challenges to the service quality due to the unpredictable evolution and the low reliability of the channel. Noise and interference are related to the non-stationary nature of the environment and with the presence of several other transmitting sources.

The main effects due to signal weakening through the medium can be summarized in two general categories:

Path Loss describes the dissipation of the emitted power in the propagation channel;

Path Shadowing includes the effects related with the emitted power absorption, reflection, diffraction and scattering by obstacles in the propagation channel.

Those are so called *large scale propagation effects* to remark the difference with respect to multi-path components interference which are referred to as *small scale propagation effects*.

The general problem is determining the shape of the electromagnetic wave incoming to the receiver knowing the emitted signal and the nature of the channel. This is obviously useful only in the very rare cases in which the channel is easy to model and presents constant properties.

The transmitted signal is a sinusoidal electromagnetic wave modulated by a function of the time that is called *complex envelope*. The **path loss** is defined as the ratio between the received and the transmitted power, expressed in dB as

$$P_L(\text{dB}) = 10 \log_{10} \frac{P_t}{P_r} \tag{2.1}$$

where P_t and P_r are respectively the transmitted and received power carried by the the electromagnetic wave. Sometimes the **path gain** is also used and it is defined as the opposite of the path loss.

The exact shape of the wave incoming to the receiver can be computed knowing the exact characteristics of the channel. In the vast majority of cases this is not possible so various approximation techniques have been developed. When the channel presents simple and regular properties, it is possible to develop physic models to approximately describe the interaction of the wave with the environment.

The strongest simplification possible consists in assuming the channel to be empty so that the transmitted waveform can freely propagate without any absorption or reflection. In this ideal case, the only part of the wave-front that interacts with the receiver is the one that propagates through the straight line between the emitter and the receiver. The problem, therefore, can be immediately simplified with a one-dimensional formulation; the channel model associated with this transmission is called a line-of-sight (LOS) channel, and the corresponding received signal is called the LOS signal or ray. The only aspect that highlights the difference with a mono-dimensional wave is the attenuation of the signal, proportional to the square of the distance spanned by the signal.

In many realistic settings in which the radio signal is subjected to multiple reflections and other scattering phenomena, it is possible to separately consider each of the components of the wave-front that reaches the receiver. Each one of these components, called *multi-path signal components*, can be described considering uniquely the mono-dimensional path connecting the source to the various reflecting surfaces to the receiver with no need to consider the evolution of the whole wave-front. That allows using simple geometric arguments instead of solving numerically the Maxwell equations given the boundary information.

It is important to notice that this model is capable of good performance whenever the position and the characteristic of the reflecting surfaces are known in each moment.

If those quantity can evolve unpredictably through time it is necessary to rely on some statistical approximations to characterize the received signal.

Several models have been developed to describe different environments that are typically encountered when dealing with channel behaviour prediction like the *Two-Rays Model*, used in urban scenarios when a single ground reflection dominates the multi-path effect, and the *Dielectric Canyon*, used in urban environments.

2.1.1 Path Loss Models

Accurate analysis of the signal propagation is possible using complex ray-tracing models or employing empirical measures. Nevertheless, results are approximated and specifically tailored for the analyzed scenario. For a general analysis of a certain architecture performance, a more convenient solution is developing a simplified model that captures the essential evolution of the signal in a general real-use scenario. The *Simplified Path Loss Model* is the most simple one and tries to capture the essential behavior of the signal attenuation in a few parameters. In all those cases in which the environment is too elaborate for the Simplified Path Loss Model to provide good results, several empirical path loss models have been developed.

Simplified Path Loss Model

The *Simplified Path Loss Model* is a model generally used to describe the attenuation of the signal, it consists in a simple law depending on a few parameters

$$P_r = P_t K \left(\frac{d_0}{d}\right)^{\gamma} \tag{2.2}$$

where K is a unit-less constant which depends on the antenna characteristics and the average channel attenuation, d is the distance at which the signal is observed and d_0 is a reference distance for the antenna far-field.

The attenuation (in dB) is therefore:

$$P_r(\text{dBm}) = P_t((\text{dBm}) + K(\text{dB}) - 10\gamma \log_{10}\left[\frac{d}{d_0}\right] . \tag{2.3}$$

The model is a good approximation of the real experimental results when d is sensibly greater than d_0. The constant γ is called *path loss exponent* and assumes different values according to the complexity of the environment in which the signal travels and to the frequency of the signal itself. Therefore, despite the value for γ in the free-space model is always 2, in typical applications it lies between 3.6 and 5.1 in a

Non-Line-of-Sight (NLoS) mobile-to-mobile environment [Turkka and Renfors, 2008]. Therefore, the signal attenuates exponentially with a high coefficient and transmitting at high distances might become challenging. Nevertheless, adopting a multi-hop topology in order to reduce the distances crossed by the signal is not feasible. As explained in [Tuset-Peiro et al., 2013] multi-hop links are complex to manage because they require some degree of synchronization among the involved devices, and the execution of routing protocols to determine and update the routes between any end device and its intended destination becomes necessary.

Indoor Empirical Models

More recently the problem of describing the path loss in indoor environment has been addressed. It is difficult to express in a general form since indoor environment can differ widely in size, shape and materials. The reflection and absorption effects also depend on the frequency of the signal and many investigations have been carried out to explore the attenuation effect of walls and floors to a signal of specified frequency. As an indicative quantity it can be reported the value of 10-20dB of attenuation for a signal at 900MHz passing through a floor in a building. Increasing the number of floors makes the attenuation due to the last of them more and more weak up to a few decibels).

Also the material of the partition must be taken into account. Even if measurements taken by different researchers may vary significantly, an indicative information can be kept. In Table 2.1 the partition loss is measured at 900-1300MHz for different materials resulting in the following data.

Partition Type	Partition Loss (dB)
Cloth Partition	1.4
Double Plasterboard Wall	3.4
Foil Insulation	3.9
Concrete Wall	20.4
All Metal	26

Table 2.1: Typical Partition Losses depending on the partition structure and material.

As said, it is difficult to provide a precise confidence interval for the Partition Loss value but it is possible to observe a qualitative difference between the various partitions types. The metallic partition is by far the one presenting the highest partition loss between the analyzed ones, followed by the concrete. This remarks

the relevance of the materials used to build a specific indoor environment. For an industrial setting, the abundance of metal and concrete makes the environment one of the most challenging with regard to the signal attenuation.

A simple way to integrate the effect of walls and generic partitions into the path loss computation is to modify the simple path loss model by adding two additional terms representing the floor attenuation factor and the partition attenuation factor for each of the floors and the partitions traversed by the signal.

The last effect worthy of being cited is the penetration loss due to the penetration of the signal inside the indoor environment in the case in which the antenna is placed outside the building.

2.1.2 Shadow Fading

Path loss represents the mean effect of the absorption and reflection of the wave-front with the various obstacles that can interfere with the signal propagation. In addition to that, variations of the signal due to slightly different paths result in an effect known as *shadow fading*. Since the exact positions, shapes and dielectric properties of the obstacles cannot be always determined exactly and, even if this was possible, it may require an excessive computational cost to exactly simulate the environment, a statistical model is often used to concisely describe the environment properties both in indoors and outdoors scenarios.

The distribution from the which the path loss is sampled out is a *log-normal* distribution. The mean value is usually referred to as average path loss, empirical measurements for this value range between 4 and 12 dB. The apparent awkwardness of the log-normal distribution is due to the logarithmic transformation used to express the path loss in Decibel.

A simple justification of this model can be based on the fact that a signal that traverses a number of objects faces an attenuation of $s = ce^{-\alpha \sum_i d_i} = ce^{-\alpha d_t}$, where d_i depend on the specific shape and dielectric properties of the objects. in a situation in which the number of objects is large, d_t can be treated ad a Gaussian random variable and $\log(s)$ will have a Gaussian distribution as well. The shadow fading and the path loss find a natural way to be combined by including the mean of the shadow fading into the path loss (constant) term thus describing the shadow fading as a Gaussian variable of mean zero.

This formalism is used to compute the *outage probability* i.e. the probability for a receiver to sense a signal of power higher than a minimum level below which performance is considered to be unacceptable and thus to design the structure of a wireless network to guarantee the minimum power level in each point of interest with

a specified minimum probability.

2.1.3 Multi-path Channel Models

In this section fading models for the constructive and destructive addition of different multi-path components introduced by the channel are examined. Deterministic models are rarely available, a statistical characterization of the channel is required to fit solutions that can evolve through time or not be entirely known.

In the analysis of the effects due to the superposition of different multi-path components, two important effects arises presenting different time scales:

- fast channel variations happens when delay between different multi-path components could be noticeable with respect to the inverse of the channel bandwidth;
- slow channel variations happens time-varying nature of the multi-path channel due to a movement of the of either the transmitter of the receiver.

To better understand how these effects are generated and how they impact the final received signal, let's start by analysing the transformations that occur in the propagation of the wave-front in the channel.

Given the transmitted signal, the received signal is reconstructed by summing (with an obvious generalization in the continuum case) all the terms modified by the propagation of the wave-front in the channel. A convenient way to express the resulting signal is summing all the *resolvable multi-path components* which correspond to the multi-paths associated with similar scattering events and, therefore, cannot be separated by the receiver. In more detail, two multi-path components with delay τ_1 and τ_2 are resolvable if their delay difference is significantly greater than the inverse of the signal bandwidth, otherwise are said to be non-resolvable. All the non-resolvable components are seen by the receiver as a single wave-front and are combined into a single multi-path component with delay $\tau \approx \tau_1 \approx \tau_2$ with a perturbation in phase and amplitude due to the specific path and interactions. Typically, these combined components undergo fast variations due to slight differences in the paths that result in sudden variations of the received signal called *fast fading* to differentiate them from the channel variations due to some modification of the environment crossed by the waveform, that are referred to as *slow fading*.

Even though fast fading cannot be predicted and generates a sudden variation in the channel between two consecutive transmission attempts, slow fading can be regular enough to allow to exploit the previous history of the channel to infer information about future channel states.

Depending on the spread of time delays between different non-resolvable components, two different models are introduced:

- if the channel delay spread is small, then the LOS and all multi-path components are typically non-resolvable, leading to the *narrow-band fading model*;
- if the delay spread is large, then the LOS and all multi-path components are typically resolvable, leading to the *wide-band fading model*.

2.2 Interference in Wireless Networks

Interference is well known problem in the unlicensed bands used by wireless LANs (WLANs), and is an increasing challenge in all kind of WLAN environments. Interference in WLAN applications leads to a reduction in data-traffic throughput as well as a reduction in the effective communication range. This is particularly critical for human-like communications (voice and video applications) causing a bad user experience of service (EoS), but in the worst cases can also include the temporary failure of a given link, thus affecting severely any kind of communication. As the number of unlicensed devices grows and as ever more mission-critical applications are deployed on WLANs, interference represents a challenge that must be addressed. With the unlicensed bands available to many devices beyond WLANs, these potential sources of interference are, like WLANs themselves, increasing in number. This presentation follows the White Paper released in 2010 by Cisco [CISCO, 2010], one of the most important players in the field of IoT and wireless communications.

In particular, Radio-Frequency Interference (RFI) is a major problem in the deployment and use of WLANs that operate in the unlicensed bands like the one analyzed in this work. The unlicensed band is a spectrum band reserved by regulators worldwide for applications without any requirement for the individual user. This is a big advantage for the ease of installation and the absence of costs to transmit in this band but, at the same time, a potentially large number of wireless devices may be competing to transmit in the same frequency in a particular location. This can lead to interference and thus degraded user connectivity in terms of throughput, link quality, and range.

As consequence of the lack of restriction for the number of devices that can transmit in the unlicensed band, devices operating in this band should accept any interference that may be present. Even if it is possible to attack a wireless network by generating a strong signal in the same operational bandwidth (jamming), this phenomenon is rarely encountered and interference in the unlicensed bands is usually

unintentional and due to other devices operating legally in this band. Interference may also arise from licensed services, including amateur radio equipment, RADAR systems, and many other devices allowed to operate at much higher power than their unlicensed counterparts.

From a more technical point of view, interference occurs when two radio signals with sufficient proximity to each other are transmitted on the same frequency at the same time. Interference can can affect simultaneously multiple signals that present similar transmit power, and so it is likely that they can mutually interfere. Otherwise if one signal has greater power than the others present in the same bandwidth, weaker signals will suffer interference from the stronger, which instead won't be affected significantly.

As explained in the previous section, the attenuation of the signal of radio waves decreases polinomially with the distance with a coefficient that is 2 in open spaces but can assume higher values in indoor environments. Therefore the intensity of a radio signal may decrease strongly while moving from transmitter to receiver, causing the signal to change from interferer to interferee with respect to an other other signal that experience a different power variation.

Interference is not only a function of relative power but also depends on the transmit duty cycle. The higher percentage of time that a given device is transmitting with a large share, the greater the probability of interference. It is possible for two otherwise potentially interfering signals to "timeshare" a given frequency (in an uncoordinated fashion), resulting in relatively little mutual interference.

With respect to WLANs, as said before, interference may come from a variety of sources, in particular from other WLAN networks and from other devices that use different transmission protocols. This leads to different situations that are worthy of being analyzed separately.

- Interference from other WLAN networks can belong to two general categories: *co-channel interference* (CCI), or *adjacent-channel interference* (ACI). In the first case, the interference phenomenon interests two access points on the same channel, in the latter interests two access points operating in close proximity channels. To assess the channel freedom, WLANs adopt a "listen-before-talk" protocol, based on Carrier Sense Multiple Access with Collision Avoidance (CSMA/CA). As a consequence of that, each network waits to transmit until the channel is free and this helps the two networks to cooperatively share (even if not optimally) the channel capacity.

- Non-WLAN sources use transmission protocols different from those of WLANs. There is no verification of clean channel before transmitting and this leads

more often in a severe degradation of WLAN transmissions. The amount of non-WLAN devices operating in the unlicensed band is huge. There is a wide range of domestic use devices that exploit the unlicensed band such as Bluetooth products (some of them may operate at the same power levels as WLANs). In addition, there is a variety of industrial devices that may potentially interfere with WLANs such as wireless video surveillance cameras, wireless security and energy management systems, proprietary wireless bridges, and computer peripherals.

This distinction helps to understand a major problem in detecting and solving interference problems. Since a WLAN transceiver can only detect a WLAN signal, the radios used in WLAN networks (both on servers and clients) do not perform well in diagnosing interference due to sources external to a WLAN network. As discussed earlier in this section, the amount of non-WLAN devices commonly used both for private and entrepreneurial purposes is constantly growing. To identify these signals not generated by a WLAN it is commonly used a *spectrum analyzer*. Unfortunately this tool is quite expensive and requires some expertise to be used. Therefore it is not suitable for a network that should meet the easy of use and installation required in the problem analyzed in this work and different methods to handle the interference problem should be found.

Chapter 3

Related Work

This Chapter presents in depth the background of IEEE 802.15.4g SUN networks, comprehensive of the IEEE 802.15.4g SUN modulations used in this work, and the work related to communication reliability using diversity mechanisms and machine learning algorithms in this network type. Then, Section 3.3 presents an overview of the applications of Multi Armed Bandit based algorithms to wireless networks channel selection. This is preparatory to the introduction of the modulation selection strategies presented in Section 4.2.

3.1 IEEE 802.15.4g Standard

IEEE 802.15.4 is a technical standard which defines the operation of low-rate wireless personal area networks (LR-WPANs). It was first released in May 2003 and defining a PHY (PHYsical) layer and a MAC (Medium Access Control) layer. Recently various studies have been focused on the analysis of performance of IEEE 802.15.4g SUN (Smart Utility Network) modulations showing a rising interest in this subject.

At the physical layer, the standard employed the Direct Sequence Spread Spectrum - Offset Quadrature Phase Shift Keying (DSSS-OQPSK) modulation and provides data rates of 20 kbps and 40 kbps in the Sub-GHz bands (868 MHz in Europe, 915 MHz in America), respectively, and of 250 kbps in the 2.4 GHz band (available worldwide). The selected modulation provided a good trade-off between radio transceiver complexity, robustness, energy consumption, and communication range [Muñoz et al., 2018b]. At the MAC layer, the standard defined slotted/synchronized and unslotted/unsynchronized operation based on the CSMA/CA (Carrier Sense Multiple Access with Collision Avoidance) channel access mechanism to trade off bandwidth, latency and energy consumption of the devices.

The adoption of the IEEE 802.15.4g standard by different low-power wireless technologies has promoted the revision of the standard three times (i.e., in 2006, 2011 and 2015) in order to clarify the operation and to add new features to both the PHY and MAC layers. For example, the 2015 standard revision adopted the MAC layer proposals defined in the IEEE 802.15.4e-2012 [IEEE, 2012] amendment. This amendment defined the *Time Slotted Channel Hopping* (TSCH), a channel access mechanism that combines *Time Division Multiple Access* (TDMA) and *Frequency Division Multiple Access* (FDMA) to support industrial requirements which in the toughest cases may require reliable packet delivery up to 99.999% in adverse conditions, such as multi-path propagation and external interference. This is not an ubiquitous requirements in any industrial application; in fact in the work-case presented in the following chapters the requirement is a reliable packet delivery of 99% but in presence of extremely harsh environmental conditions.

Of particular relevance for this work is the adoption in the IEEE 802.15.4-2015 standard revision of the three new physical layers targeted to SUN (Smart Utility Network) applications, as previously defined in the IEEE 802.15.4g-2012 amendment. The modulations present different target objectives: SUN-FSK and SUN-OQPSK modulations are focused on maintaining backwards compatibility with previous standards and commercially available transceivers. SUN-OFDM, instead, is focused on robustness and spectrum efficiency at the physical layer.

In the following sections the modulations SUN-FSK, SUN-OQPSK and SUN-OFDM are described in detail, since these modulations are used to provide the channel diversity necessary to implement the modulation selection strategy.

SUN-FSK

The SUN-FSK modulation has two main advantages: the first one is the good power efficiency and the low implementation complexity, and the second one is the compatibility with legacy systems. At the same time has shown good performances in the dataset used in this work, proving to have a good reliability with respect to the other SUN modulations in harsh conditions.

An advantage of SUN-FSK modulation is its availability in different countries due to the possibility of using it in different frequency bands. For example in Europe it can be used both the 863-870 MHz and the 2.4 GHz bands. The latter is freely available worldwide.

Depending on the frequency band, different operation modes are defined. An operation mode is a protocol that specifies transmission parameters such as the modulation type (2-FSK or 4-FSK), the modulation index and the channel spacing.

Focusing on the 863–870 MHz band, which is the one used for the data acquisition process, three different data rates are supported. The data rate is specified by the selected operation mode and may assume a value of 50 kbps, 100 kbps, and 200 kbps. The 200 kbps data rate is achieved when using 4-FSK, the other two are achieved using 2-FSK.

In the deployment described in this work, the Mode 1 was used, which uses 2-FSK, with a data rate of 50 kbps. In this mode, the total number of channels is 34, with a channel spacing of 200 kHz.

SUN-OQPSK

The OQPSK modulation was introduced in the first version of the IEEE 802.15.4 standard, in 2003. It was firstly defined only for the 2.4 GHz band, providing a bit rate of 250 kbps, subsequently other frequency bands have been added. In the IEEE 802.15.4g bitrates values may vary from 6.25 to 500 kbps.

SUN-OQPSK adopts a mechanisms to handle the interference problems called Direct Sequence Spread Spectrum (DSSS). It also exists an alternative spreading mode, called Multiplexed DSSS (MDSSS).

The symbol rate is defined as the bit rate of the synchronization header (SHR). Other important parameters are defined in the the physical layer packet header (PHR), such as the spreading mode, and the rate mode. The Forward Error Correction (FEC) is always applied in the PHR field. When using DSSS as the spreading mode, FEC shall also be applied to the Physical Service Data Unit bits. For spreading mode set to MDSSS, FEC is optional, depending on the rate mode. To improve robustness, interleaving may be used in conjunction with FEC.

For each frequency band, up to four rate modes are supported, but only the rate mode 0 is mandatory. In Mode 3 of the sub-GHz bands (including 863-870 MHz), DSSS is not used for the payload, this allows to achieve a higher data rate. For the 2.4 GHz, instead, DSSS is used for the payload in all rate modes.

SUN-OFDM

The SUN-OFDM was first defined in the IEEE 802.15.4g standard, and after incorporated in the IEEE 802.15.4-2015. It present features slightly different from the other described modulation since it has been designed to provide high data rates and long range, which are not required in the specific setting considered in this work and presented in detail in Section 5.1. As a consequence of that, differently from FSK and OQPSK, OFDM have not been widely used for low-power wireless communications, due to the stringent processing, memory and energy consumption requirements. As

in the previous cases OFDM tries to be robust to interference and multi-path fading problems.

The SUN-OFDM may be used in different frequency bands (both 863-870 MHz and 2.4 GHz), and provides data rates from 50 kbps to 800 kbps. The sub-carrier spacing is constant and is equal to 10416-2/3 Hz, while the symbol rate is equal to 8-1/3 ksymbol/s (a symbol period of 120 µs).

Four different options are defined, for each option, a set of Modulation and Coding Schemes (MCS), numbered from 0 to 6, may be used. In the acquired dataset, the lowest supported MSC have been chosen for the option being used, both for SHR and PHR.

The Protocol Data Unit at Presentation Layer (PPDU) of the SUN-OFDM (which is informally referred to as a packet in the following sections) is composed by a SHR, the payload, and the PHR, that contains the information about the transmission configuration.

3.2 Reliability in IEEE 802.15.4g Networks

Diversity schemes are widely used in wireless networks to improve the communication reliability, and to deal with the temporal and spatial variations in link quality. Different strategies may be adopted in different layers. At the physical layer antenna and coding diversity are two well-established mechanisms, but they are not widely used in low-power networks as they require additional or complex hardware. At the data-link layer, packet replication in the time and frequency domains are two widely used diversity schemes thanks to their simplicity. However, packet replication increases node energy consumption and impacts network congestion, whereas frequency diversity requires time-synchronization among nodes, thus increasing complexity.

Several papers have proposed the use of diversity schemes in IEEE 802.15.4 networks. For example, the authors of [Park et al., 2010] focus on the data-link layer and propose an adaptive algorithm based on MAC (Medium Access Control) parameters (i.e., macMinBE, macMax-CSMABackoffs, and macMaxFrameRetries) for minimizing power consumption while guaranteeing reliability and delay constraints in the packet transmission. [Watteyne et al., 2009] and [Watteyne et al., 2010] proposed using time synchronization and channel hopping (i.e., sending subsequent packets over different frequency channels) at the physical layer as a means to combat both multi-path propagation and external interference. The protocol proposed in [Gomes et al., 2019] combines multi-channel communication, real-time link quality estimation, and dynamic channel allocation, to deal with the problems that affect the link quality in industrial environments.

Several recent papers have applied machine learning in IEEE 802.15.4 networks. In [Bombino et al., 2020] different supervised-learning algorithms are evaluated for the inference of the radio-link state (i.e. LoS or NLoS radio links). By monitoring the link state in real-time it is possible to dynamic adapt the transmission scheme to improve reliability. However, only the O-QPSK modulation at 2.4 GHz is considered in the evaluations, and no diversity mechanism is proposed.

Some articles already discussed in this section propose adaptive diversity strategies to improve network reliability, but they do not consider the use of multiple modulations. Modulation diversity is a method to improve the reliability of communications by using different modulations. That is, consecutive packets can be transmitted using two or more modulations (e.g., FSK or PSK), taking advantage of their different properties regarding propagation and interference effects. For example, it is well known that narrowband modulations, such as FSK, are more robust against interference, whereas wideband modulations, such as OQPSK-DSSS, provide better tolerance against multi-path propagation.

Regarding modulation diversity, some papers have applied this concept in different ways and for different purposes. In [Zubair et al., 2016], a dual mode IEEE 802.15.4 receiver is proposed. The receiver can choose between a MSK (Minimum Shift Keying) detector or a OQPSK detector to trade energy consumption, latency, and reliability. In addition, the it can define the mode based on a SNR indicator, to optimize performance. However, the authors do not consider the use of the SUN modulations, neither propose the use of different modulations to transmit the packets. In [Sousa et al., 2014] the authors propose using cooperative modulation diversity to improve reliability. In particular, nodes rotate a QPSK constellation and interleave the phase and quadrature components independently. However, this approach requires modification at the physical layer, and the use of relay nodes, which can be difficult in sparse networks. Finally, in [Savazzi et al., 2019] the authors propose using modulation diversity for LoRa networks to improve a localization algorithm. The modulation diversity is obtained by changing bandwidth, spreading factor and code rate. Overall, these papers propose the use of modulation diversity, but they do not propose or evaluate adaptive modulation selection strategies for low-power wireless networks.

In [Gomes et al., 2020] three different adaptive modulation diversity strategies are proposed, for IEEE 802.15.4g SUN networks, called *1M*, *2M*, and *3M*. These strategies use a simple link quality estimation mechanism, based on the ACK Reception Ratio. In this work, it will be compared the proposed adaptive modulation selection strategies based on MAB algorithms to the *3M* mechanism, which presents the best performance in the evaluations described in [Gomes et al., 2020].

Over the past few years several research papers have evaluated IEEE 802.15.4g networks. In [Muñoz et al., 2018], the authors evaluate all 31 physical layer configurations of the IEEE 802.15.4g for environmental observations. The results show that the longest radio links were obtained when using SUN-FSK or SUN-OQSPK, compared to SUN-OFDM. In [Muñoz et al., 2018a], the authors evaluate three IEEE 802.15.4g configurations operating at 2.4 GHz: O-QPSK, OFDM with frequency repetition, and OFDM without frequency repetition, and show that channel hopping makes sense even when using SUN-OFDM, as the channel width is small and all sub-carriers are influenced in a similar way by multipath fading. In [Muñoz et al., 2018b], the authors also evaluate the IEEE 802.15.4g using the 2.4 GHz ISM band, for smart building applications. The results show that for the considered indoor scenario, which is severely impacted by multi-path propagation, SUN-OFDM can provide better reliability than SUN-OQPSK. Overall, these papers show that the different physical layer configurations may present different levels of quality for different scenarios. However, the authors do not propose or evaluate any mechanism to deal with the different challenges of low-power wireless communications.

3.3 MAB strategies for Wireless Networks

The Multi Armed Bandit (MAB) problem consists in finding, within a set of options that gives stochastic rewards, the most profitable one. It can be effectively applied to many network problems by choosing the best channel of communication between the available ones based on some feedback provided from the environment. The advantage of this formulation is that it does not require a detailed knowledge of the environment and only exploits the channel response, thus it is easy to generalize to a variety of use cases.

In 2020 the dynamical channel selection in a IEEE802.11a-based, four-channel WLAN has been addressed by using MAB algorithms in a dynamically changing electromagnetic environment [Takeuchi et al., 2020]. In this specific application the kind of communication is different to the, and the quality of the user's experience is strongly influenced by the delay in the packets transmission. Therefore specific attention has been put into the speed of transition between channels when the environment conditions change.

In recent publications like [Taheri Javan et al., 2020], [Gomes et al., 2018], and [Dakdouk et al., 2018], MAB algorithms are used to optimize IEEE 802.15.4-TSCH (Time Slotted Channel Hopping) networks. In the first one, the scheduling problem is modeled in terms of a combinatorial MAB process, in order to compute the optimal schedule based on real-time interactions with the wireless network. In the second

one, the channel quality estimation process is modeled as a MAB problem, in order to classify the channels and manage the blacklists (i.e. the list of channels that are not allowed to be used by the nodes). In [Dakdouk et al., 2018] the authors also use MAB algorithms to select channels in TSCH networks. In [Hasegawa et al., 2020] the distributed channel selection problem is modeled as a MAB problem, to select channels in IEEE 802.15.4g networks under interference of Sigfox and LoRaWAN devices.

In addition to well known established algorithms [Sutton and Barto, 2018] new methods inspired to physical models to solve the MAB problem are getting attention. The underlying idea is that biological systems usually cope with the complexity of their decision making problems by exploiting basic physical phenomena, resulting in a much simpler and more efficient method than a classic algorithm. In particular the *Amoeba* reaction to external stimuli has inspired a method that consists in manipulating an in-compressible fluid straining it towards points in the space that represent possible actions. The resulting algorithm is called *tug-of-war* (TOW) [Kim and Aono, 2015]. Also photonic behaviour has been studied to address the problem of competitive MAB (CMAB) i.e. maximizing the social rewards of a set of players while ensuring equality [Chauvet et al., 2019].

Chapter 4

Proposed Methods

This section presents the two mechanisms proposed in this work to improve the channel reliability: the *re-transmission shaping* and the *modulation selection* strategies. The role of the re-transmission shaping is to efficiently determine the maximum number of re-transmissions for each packet, regardless the modulation used to transmit it. The modulation selection, instead, aims to provide the best modulation to transmit each packet for each re-transmission attempt. Therefore, these two strategies address complementary tasks. After a detailed description of both the mechanisms, it is also discussed their combined implementation.

4.1 Re-transmission Shaping

Re-transmissions are a common mechanism used at the data-link layer to guarantee the delivery of data packets between an end-device and a gateway using a wireless communication technology. Whenever the acknowledgment packet from the gateway is not received at the end-device due to physical layer effects (i.e., multi-path propagation or internal/external interference), the end-device will re-transmit the original data packet again to provide another opportunity for the packet to be successfully received at the gateway. However, since physical layer effects are not deterministic and packet re-transmission increases end-device energy consumption and network load, a maximum number of re-transmissions per data packet is typically set. But assigning a fixed number of re-transmissions per packet may not be optimal, as if channel conditions are too adverse, the originating end-device could need more than the fixed number of re-transmissions to deliver a data packet and, hence, this would be lost.

Taking that into account, the aim of the re-transmission shaping mechanism that we present in this section is to dynamically adapt the number of maximum

re-transmissions per packet according to channel conditions in order to meet both the data delivery requirements of the application and the target battery lifetime of end-devices. That is, given the average number of re-transmissions per data packet, the re-transmission shaping mechanism keeps track of the number of re-transmissions that have not been used to transmit previous data packets (i.e., if packets have been received by the gateway at the first transmission attempt). These unused re-transmission attempts are accumulated and can be used in the future when channel conditions are bad and the average number of re-transmissions per data packet is not sufficient to guarantee successful delivery.

Considering this high-level description, we now focus on presenting the system model that defines how re-transmission shaping operates. For that, we assume that we have a network with n end-devices, with a battery of capacity C (mAh) that transmit a data packet with length L (bytes) and period T (seconds), and one gateway that receives the packets transmitted by end-devices. Upon successfully receiving a data packet from any end-device the gateway transmits an acknowledgment packet (ACK) back to the originating end-device. If the originating end-device does not receive the acknowledgment packet, either because the original data packet is not successfully received or the acknowledgment packet is lost, then the originating end-device re-transmits the data packet.

Considering the values of C, L and T, the average number of re-transmissions per data packet is N_{AVERAGE} and we assume that it is set to a value that allows to meet the battery lifetime of the device. That is, if N_{AVERAGE}=3 the device is allowed to perform 3 re-transmissions per data packet while operating for 1 year[1]. Then, when the source end-device succeeds in transmitting a data packet i with a number X_i of re-transmissions, being $0 \leq X_i < N_{\text{AVERAGE}}$, the number $U_i = N_{\text{AVERAGE}} - X_i$ of unused re-transmissions can be accumulated for the re-transmission of subsequent data packets.

Hence, as depicted in Figure 4.1, the model of the re-transmission shaping mechanism is based on 5 variables N_{AVERAGE}, N_{MAXIMUM}, N_{ALLOWED}, N_{USED} and $N_{\text{AVAILABLE}}$, as described next:

- N_{AVERAGE} is an input value that represents the average number of re-transmissions per data packet that are allowed while ensuring the lifetime of the end-device. It is not required to be an integer, it can be directly derived from the device power constraint.

[1]Of course, the exact values will depend on C, L and T, as well as the voltage and the transmit/receive current consumption of the radio transceiver, and the battery capacity, among others, but this discussion is out of the scope of the paper.

- N_{MAXIMUM} is an input value that represents the number of extra re-transmissions per packet that are allowed in addition to N_{AVERAGE}.
- N_{ALLOWED} is an output value that represents the maximum number of re-transmissions that are allowed for the current data packet being transmitted.
- N_{USED} is an input value that represents the number of re-transmissions that have been required to successfully deliver the previous data packet to the gateway.
- $N_{\text{AVAILABLE}}$ is an internal state variable that accumulates the number of re-transmissions that have not been spent in previous data packet transmissions and, hence, can be used in the future. It is initialized to zero.

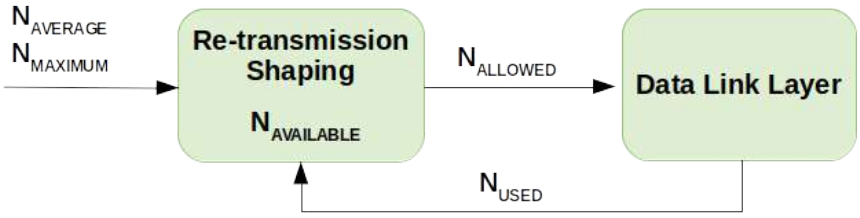

Figure 4.1: Diagram of the re-transmission shaping mechanism with the input (N_{AVERAGE}, N_{MAXIMUM} and N_{USED}), output (N_{ALLOWED}) and the internal state ($N_{\text{AVAILABLE}}$) variables, and its relationship with the data-link layer.

Regarding N_{MAXIMUM}, notice that its value is set to avoid a given packet transmission that experiences bad instantaneous channel conditions to deplete all the N_{ALLOWED} re-transmissions available. Hence, its value has to be set depending on the context of each deployment. For environments presenting short deep drops in the link reliability it can be set to a high value, allowing to strongly increase the number of re-transmissions for short periods of time. In contrast, for environments with long shallow drops in link reliability it can be set to a low value, allowing to extend the effects of re-transmission shaping for a longer period of time.

Using these variables, the operating principle of the re-transmission shaping mechanism is the following. Before a data packet transmission starts, the re-transmission shaping mechanism calculates the N_{ALLOWED} of re-transmissions available as

$$N_{\text{ALLOWED}}(k) = \text{floor}(N_{\text{AVERAGE}} + \min\{N_{\text{AVAILABLE}}(k), N_{\text{MAXIMUM}}\}). \tag{4.1}$$

so that, if unused re-transmissions are available, they are added to N_{AVERAGE} without exceeding the threshold set by N_{MAXIMUM}.

The N_{ALLOWED} value is then used by the physical layer to perform re-transmissions until the data packet is either successfully received (i.e., including the acknowledgment) or the number of re-transmissions becomes zero and no more re-transmissions can be performed. In either case, the re-transmission shaping module receives the number N_{USED} of re-transmissions used for that particular data packet and performs the following operation to update the internal $N_{\text{AVAILABLE}}$ variable:

$$N_{\text{AVAILABLE}}(k+1) = N_{\text{AVAILABLE}}(k) + (N_{\text{AVERAGE}} - N_{\text{USED}}(k)). \tag{4.2}$$

Notice that it cannot be negative because N_{USED} is always lower than N_{ALLOWED}, which depends on $N_{\text{AVAILABLE}}$ as in Equation 4.1.

Since in the first iteration $N_{\text{AVAILABLE}} = 0$, the formula that expresses $N_{\text{AVAILABLE}}$ for a generic time step k is

$$N_{\text{AVAILABLE}}(k) = \sum_{i=0}^{k-1} (N_{\text{AVERAGE}}(i) - N_{\text{USED}}(i)). \tag{4.3}$$

Notice that using these variables, the re-transmission shaping mechanism can emulate the usual re-transmissions strategy where N_{AVERAGE} is set to a constant value per data packet. This behavior can be achieved by setting N_{AVERAGE} to an integer value and making N_{MAXIMUM} equal to zero. In that case, for every data packet transmission the maximum number of re-transmission attempts is constantly equal to N_{AVERAGE}. In this case, the re-transmission shaping mechanism does not perform any additional task to the basic fixed number of re-transmissions case. In fact, as it can be noticed from Equation 4.1, despite $N_{\text{AVAILABLE}}$ increases, the value of N_{ALLOWED} is always upper bounded by N_{AVERAGE}. Hereinafter, we will refer to the particular case in which N_{MAXIMUM} is set to zero as *no re-transmission shaping* (i.e., noRS), as this represents the base scenario that allows to compare the performance gains of our proposal.

4.2 Modulation Selection

Whenever a variety of mechanisms are available to transmit data packets between a gateway and an end-device, a natural way of improving the network reliability is adopting for each packet transmission the mechanism that presents the higher probability of successfully delivery. In the current framework the different transmission

mechanisms consist in the SUN modulations presented in Section 3.1. The randomness of the channel evolution makes impossible to predict the most convenient modulation on theoretical basis, it is possible instead to exploit the history of the transmission attempts to estimate in each time the best modulation. This can be done by keeping track of the acknowledgment received by the end-device from the gateway for each transmission attempt made with a specific modulation.

The exact form in which the best strategy computation has been performed will be presented later in this chapter, now the focus is on the high level implementation of the strategies by considering the actual modulation selection mechanism as a black box and discussing the interaction of the model with the channel. As depicted in Figure 4.2, for each transmission attempt k the selected modulation MOD_K is used to transmit the packet. The gateway sends an aknowledgement (ACK) to the end-device whenever it receives a packet. It should be noticed, however, that the ACK reception by the end-device is subject to the status of channel reliability. Therefore it is possible that, even if the packet is received by the gateway, no ACK reaches the end-device and the transmission is erroneously considered as unsuccessful. Each packet can be re-transmitted N_{AVERAGE} times in order to increase the transmission probability, therefore this value is given in input to the modulation selector module.

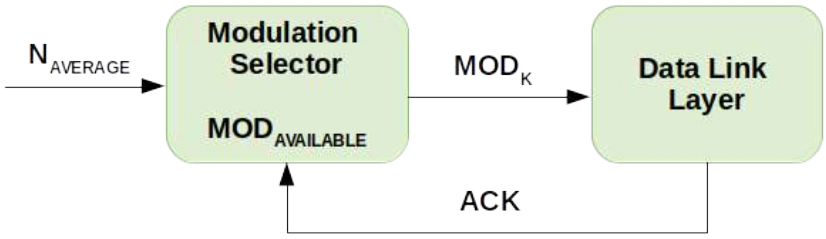

Figure 4.2: Diagram of the modulation selection mechanism with input (N_{AVERAGE}, ACK) and output variables (MOD_K) and internal state (list of available modulations $\text{MOD}_{\text{AVAILABLE}}$ with an associated quality score).

4.2.1 Restless Multi Armed Bandit Problem

The problem of recurrently choosing an action from a (finite or infinite) set based on the expected reward that the action will produce has been widely studied and formalized in the model known as Multi Armed Bandit (MAB) problem.

In its most basic formulation, a K-armed bandit problem is defined by random variables $X_{i,n}$ for $1 \leq i \leq K$ and $n \geq 1$, where i is the index of a gambling machine (i.e., the "arm" of a bandit) and n is the index of the iteration of plays of the machine. Rewards obtained by different plays of a machine are independent and identically distributed according to an unknown probability measure with unknown expectation μ_i. In general each machine has a different probability measure associated. Also rewards obtained by different machines $X_{i,s}$ and $X_{j,t}$ are independent for each $1 \leq i, j \leq K$ and each $s, t \geq 1$.

A *policy*, or *allocation strategy*, A is a function that specifies the machine to play depending on the sequence of past plays and obtained rewards. Let $T_i(n)$ be the number of times machine i has been played by A during the first n plays. The *expectation regret* of A after n plays $R^E(n)$ is the expected loss due to the fact that the policy does not always play the best machine; it is defined as

$$R^E(n) := n\mu^* - \mu_j \sum_{j=1}^{K} \mathbb{E}[T_j(n)] \quad \text{where} \quad \mu^* = \max_{1 \leq i \leq K} \mu_i \, . \tag{4.4}$$

so it corresponds to the maximum possible reward minus the expected one obtained in the first n plays, conditional on all contextual variables, with expectation taken over repeated plays of an arm at a fixed point in time.

In [Lai and Robbins, 1985] it is shown how

$$\mathbb{E}(T_j(n)) \geq \frac{\log(n)}{D(p_k||p^*)} \tag{4.5}$$

where $D(p_j||p^*)$ is the Kullback-Leibler divergence between the reward probability density of the suboptimal arm p_k and the reward probability density of the optimal arm p^*. Therefore the regret grows at least logarithmically, that is, $R^E(n) = \Omega(\log n)$ and an algorithm is said to solve the multi-armed bandit problem if it can match this lower bound, i.e. if $R^E(n) = O(\log n)$.

These algorithms work by associating a quantity called *upper confidence index* to each machine. The computation of this index is not trivial: it relies on the entire sequence of rewards obtained so far from a given machine. Once the index for each machine is computed, the policy uses it as an estimate for the corresponding reward expectation, picking for the next play the machine with the current highest index.

The previous description, however, assumes that rewards obtained by different plays of a same machine are identically distributed, that means that the the underlying distribution are stationary. This approximation does not always fit the experimental conditions, the framework in which the reward distributions are not stationary is called *Restless Multi Armed Bandit*.

A known behaviour that leads to non-stationarity is due to the presence of *change-points* in correspondence of whom the distribution presents an abrupt change. The Adapt-EvE algorithm [Hartland et al., 2011] uses the Page-Hinckley test to identify change-points and add a *meta bandit* with two arms that controls the MAB algorithm that actually chooses the arm of the problem (the Adapt-EvE implementation uses UCB algorithm described in the following section but the same approach can be applied to other algorithms). The meta bandit algorithm decides if to keep the learned parameters of UCB or to restart it from scratch. This approach is capable of good performance but it is unfeasible in the scenario analyzed in this work as the evolution of the rewards distribution varies constantly.

In the dataset described in Section 5.1, however, the non-stationarity is due to a series of unpredictable changes in the channel as explained in Chapter 2 and there is no satisfactory way to describe the modulation quality evolution by means of the change-points model. In this scenario it lacks a comprehensive mathematical formulation as well as convergence results for the algorithms that can be applied. Therefore the most straightforward approach consists in exploring the performances of the most known algorithms for the non-stationary case to investigate how they perform in the specific setting, without relying on theoretical results for convergence speed.

4.2.2 Algorithms

Among the variety of algorithms that can be used to address the problem of selecting the best arm in a MAB framework, we have selected some of the most known between the ones that present a low computational charge. In fact these solutions are meant to be deployed in real case scenarios in which the power drain of the sensor is a crucial aspect to evaluate the effectiveness of the implementation. In the rest of this section the selected algorithms will be presented in the general form; in this specific case however the possible *actions* coincide with the SUN modulations and the reward assumes only the values 0 and 1 accordingly to the transmission outcome and to the reception of the ACK by the end-device.

Epsilon-greedy

The epsilon-greedy policy (EG) is a widely used algorithm in Reinforcement Learning problems [Sutton and Barto, 2018]. It is based on a simple heuristic: given an arbitrary value $\varepsilon \in [0; 1]$, in each round the arm with maximum expected utility is selected with probability 1-ε, otherwise an arm is chosen with random probability

among the whole action space without consideration for the estimated values of the arms. The value of each action is computed recursively as

$$Q_{t+1}(a) = Q_t(a) + \alpha(R_{t,a} - Q_t(a)) \tag{4.6}$$

were $R_{t,a}$ is the reward at round t having played arm a and $\alpha \in (0; 1]$ is the learning coefficient that is kept fixed. In this way, from 4.6 we have that

$$Q_{t+1}(a) = (1-\alpha)^t Q_1(a) + \sum_{i=1}^{t} \alpha(1-\alpha)^{t-1} R_{i,a} \tag{4.7}$$

thus the effect of rewards decreases exponentially with the number of rounds and the policy is able to adapt to the evolution of the environment. The higher the value of α, the faster the old rewards are ignored in favour of more recent information.

Algorithm 1 Epsilon-Greedy Policy

```
Define the set of possible actions A
Define a map from a ∈ A to its value Q_0(a)
Set value for ε ∈ (0; 1) and stepsize α
for t from 0 to t_max do
    Sample ξ from U_[0;1]
    if ξ ≥ ε then
        Set â equal to argmax_{a∈A}(Q_t(a))
    else
        Randomly sample â from A
    Get the reward R_t
    Set Q_{t+1} equal to Q_t
    Set Q_{t+1}(â) equal to Q_t(â) + α(R_t − Q_t(â))
```

Softmax

The second considered algorithm is softmax also known as *Boltzmann Exploration*(BE). It consists in sequentially choosing for each round t one arm a from the Boltzmann distribution

$$P_t(a) = \frac{\exp(\tau Q_t(a))}{\sum_{a' \in A} \exp(\tau Q_t(a'))} \tag{4.8}$$

where $Q_t(a)$ is the expected value of the arm a at round t and τ is a parameter that defines the randomness of the choice and, from a physical analogy, it can be

referred to as the *inverse temperature* of the system. For τ equal to zero the choice is completely random while for τ approaching infinity the sampler tends to chose each time the arm presenting the highest empirical average, thus renouncing to the exploration phase. In [Cesa-Bianchi et al., 2017] it is highlighted the importance of choosing a suitable evolution scheme for the parameter τ as function of time; however those theoretical results hold for a stationary MAB problem and can not be used to address the non stationary version of the problem.

Algorithm 2 Softmax

1: Define the set of possible actions A
2: Define a map from $a \in A$ to its value $Q_0(a)$
3: Set value for $\tau \in (0; 1)$ and stepsize α
4: Initialize $Q_0(a) = 1 \quad \forall a \in A$
5: **for** t from 0 to $t_{\max}$ **do**
6: Set $B(a) = \frac{\exp(Q(a)/\tau)}{\sum_{a' \in A} \exp(Q(a')/\tau)} \quad \forall a \in A$
7: Sample $\hat{a}$ from A with probability B
8: Get the reward R_t
9: Set Q_{t+1} equal to Q_t
10: Set $Q_{t+1}(\hat{a})$ equal to $Q_t(\hat{a}) + \alpha(R_t - Q_t(\hat{a}))$

Upper Confidence Bound

The last policy that we have implemented is the Upper Confidence Bound action selection (UCB). This policy aims to choose every time an action considering the expected value and the uncertainty of the estimate. If an action has been explored a very limited number of times, it could be worthy to be explored again even if the estimated value is lower than other actions. The UCB policy consists, therefore, in choosing in each stage the action that maximizes a function of the expected values and the number of tries

$$a_t = \text{argmax}_{a \in A} \left[Q_t(a) + \sqrt{\frac{2 \log t}{N_t(a)}} \right] \tag{4.9}$$

where $N_t(a)$ is the number of times in which action a has been selected and the function that is added to $Q_t(a)$ is referred to as *padding function*. the argument of the argmax function is called *index* of the arm a. This approach presents some obvious problem in the non stationary case, in fact, even if an action has been widely

explored, it doesn't mean that we have reliable information about its behaviour in a subsequent stage. Therefore the relevance of old exploration should be reduced with the number of stages. Two methods have been implemented to achieve this goal: the discounted UCB (D-UPB) and the sliding window UCB (SW-UCB) approaches.

In the first one the actions counter is computed recursively applying a discount factor defined by a coefficient γ as

$$N_{t+1}(\bar{a}) = \gamma N_t(\bar{a}) + \delta^{\bar{a}}_{a_{t+1}}. \tag{4.10}$$

Algorithm 3 Discounted UCB

Define the set of possible actions A
Set value for γ in $(0; 1)$
Initialize $Q(a) = 1$ and $N(a) = 0 \quad \forall a \in A$
for t from 0 to $t_{\max}$ **do**
    for $a \in A$ **do**
        if N(a)=0 **then** $P(a) = +\infty$
        else $P(a) = Q(a) + \sqrt{\frac{2\log(n)}{N(a)}}$
$\hat{a} = \arg\max(P(a))$
Get the reward R_t
Set $Q(\hat{a})$ equal to $\gamma Q(\hat{a}) + R_t$
Set $N(a)$ equal to $\gamma N(a) \quad \forall a \neq \hat{a}$
Set $N(\hat{a})$ equal to $\gamma N(\hat{a}) + 1$

The SW-UCB is similar and consider only those action performed in the last τ stages as relevant for evaluating the function used to choose the action as in 4.9. It can be interpreted as a hard version of D-UCB since it cuts the experience accumulated before a time delay τ while in the previous case the relevance of old rewards decreases exponentially thus becoming negligible after some iterations.

Since the two approaches have shown fairly identical results, only D-UCB have been used for results presentation.

Note that in the stationary version of this algorithm $Q_t(a)$ corresponds approximately to $\mu_a N_t(a)$. Therefore the algorithm without the padding function would pick the arm a if μ_a is big and the number of times it has been explored is big enough. The presence of the padding function indeed helps to choose the arm a when the number of times the action has been explored is too small.

4.3 Combined Methods

Once defined the two proposed mechanisms to increment the channel reliability it is natural to think about applying the two methods at the same time to further increase the channel reliability. In Figure 4.3 it is represented the diagram of the combined methods. Once presented the two methods individually it is easy to understand their combined implementation: from the perspective of the re-transmission shaping mechanism, the modulation selection mechanism is just part of the packet transmission details handled by the data link layer block. The modulation selector block, similarly, is completely agnostic to the choice of the number of re-transmission for a specific packet, it takes this value as input and keep re-transmitting the current packet accordingly until an ACK is received. The implementation details of the two methods therefore are not influenced by their joint deployment. The only difference with the description done in the previous sections consists in the value of N_{USED} outputted by the modulation selector block and storing the number of re-transmission performed before receiving an ACK or before reaching the maximum re-transmissions value specified by $N_{MAXIMUM}$.

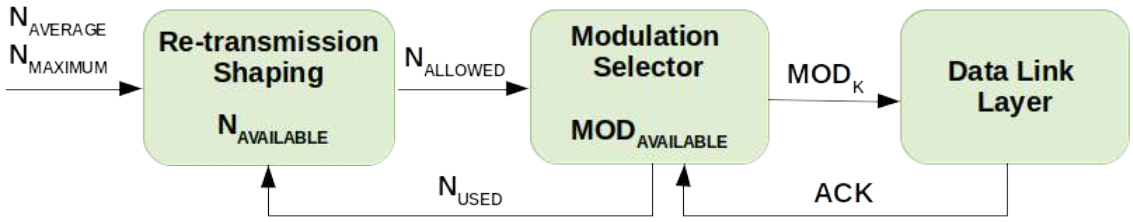

Figure 4.3: Diagram of the final architecture obtained by deploying the two proposed methods.

Chapter 5

Evaluation Methodology

This chapter introduces the dataset, the simulator, the metrics and the parameters that used to evaluate the modulation selection strategies and the re-transmission shaping mechanism described in the previous chapter.

5.1 Data Acquisition

The proposed methods have been tested using data gathered in 2020 with the specific purpose of exploring the capabilities of IEEE 802.15.4g in an challenging industrial scenario [Tuset-Peiró et al., 2020c]. A network of 11 sensor nodes and 1 gateway has been deployed in a warehouse located in Madrid (Spain). The warehouse is built with steel and concrete, as illustrated in Figure 5.1, and measures 451m $\times$ 244m. The influence of steel in the reflection and multi-path propagation effects have been introduced in Chapter 2. In such a industrial setting the presence of external sources of interference, as other other networks operating in the same band (i.e., 868 MHz), is highly probable. Finally, the presence of machinery moving across the warehouse constantly modifies the signal propagation effects, thus making the environment particularly challenging.

Regarding the specific deployment of the network, the nodes location is depicted in Figure 5.2: the gateway has been located near the warehouse entrance, whereas the nodes have been placed at different distances and heights. In particular nodes `5599`, `55DD`, `5565` and `560B` have been placed on the same vertical line but at different heights thus resulting in different distance and path propagation to the gateway.

Table 5.1 shows the node identifiers (last two bytes of the EUI-64 address) and the distance to the gateway, which is comprised between 34.0 meters and 273.5 meters.

The details of the hardware implementation of the network are represented in

(a) (b) (c)

Figure 5.1: Examples of the warehouse environment.

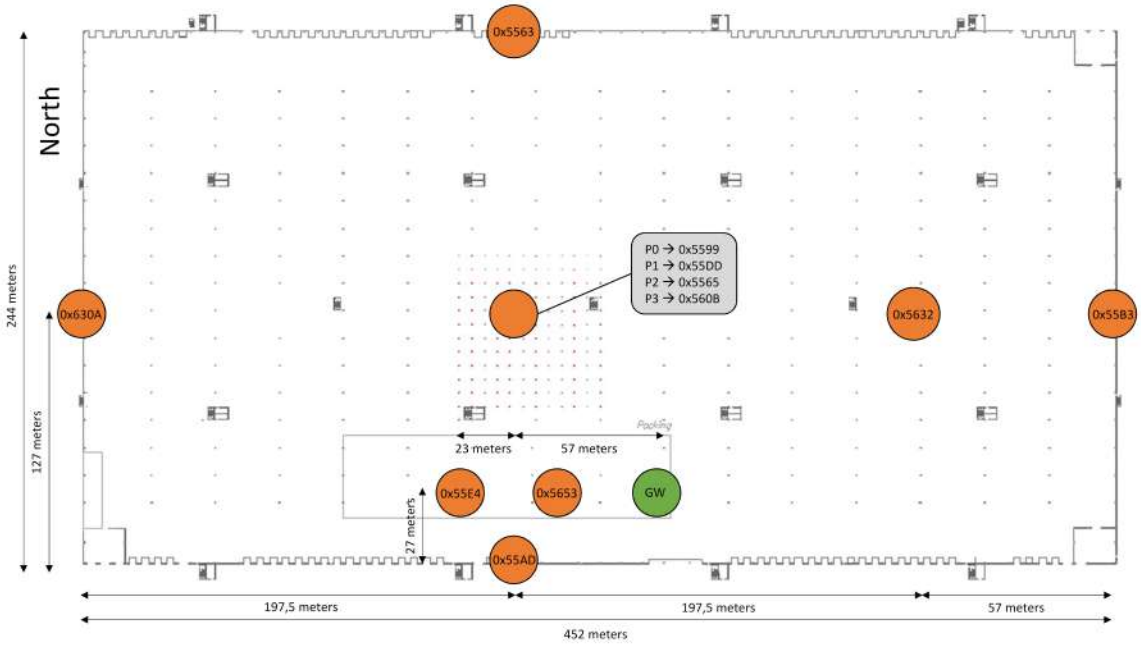

Figure 5.2: Map of the warehouse with the position of the sensors nodes (orange) and the gateway (green).

Node ID	distance (m)	height (m)
56-53	34.0	12.0
55-AD	63.0	2.0
55-E4	80.0	6.0
55-99	115.1	2.0
55-DD	115.1	6.0
55-65	115.1	10.0
55-65	115.1	14.0
56-32	172.5	2.0
55-B3	221.4	2.0
55-63	224.4	2.0
63-0A	273.5	2.0

Table 5.1: Nodes identifiers, horizontal distance to the gateway and height.

Figure 5.3, where the nodes are represented by the circles on the left and the gateway with Internet access is shown on the right. The sensors transmits every minute the retrieved environmental variables. The active sensing and transmitting time is 1750 ms, as depicted in Figure 5.4, resulting in an active time ratio of 2.9%. During the active period the nodes sample the environmental sensors (100 ms) and then perform 3 transmit cycles. At each transmit cycle the node transmits 3 different packets, one with each of the SUN modulations (i.e., SUN-FSK, SUN-OQPSK and SUN-OFDM). Between two consecutive packets in a transmit cycle there is a 50 ms inter-packet delay. Also, between the 1st and 2nd cycle there is a 100 ms delay, whereas between the 2nd and 3rd cycle there is a 200 ms delay. That is, the interference between different nodes can be safely assumed as negligible, also considering the small number of transmitting devices.

Nodes are equipped with a mechanism to reduce the number of lost packets by sensing the frequency bandwidth used to transmit before the transmission in order to check if the noise level in the channel is low enough to transmit safely. Before each packet transmission, therefore, the sensing nodes execute a CSMA/CA (Carrier Sense Multiple Access/Collision Avoidance) protocol with CCA (Clear Channel Assessment) to determine if the channel is busy. If the noise level (energy present in the channel) is below a threshold specified for the modulation in use, the CSMA/CA succeeds and the packet is loaded to the radio transceiver and transmitted subsequently. Otherwise, if the energy is above the specified threshold, the transmission is delayed for a random time between 0 and 10 ms. This check is iteratively done until the noise level in

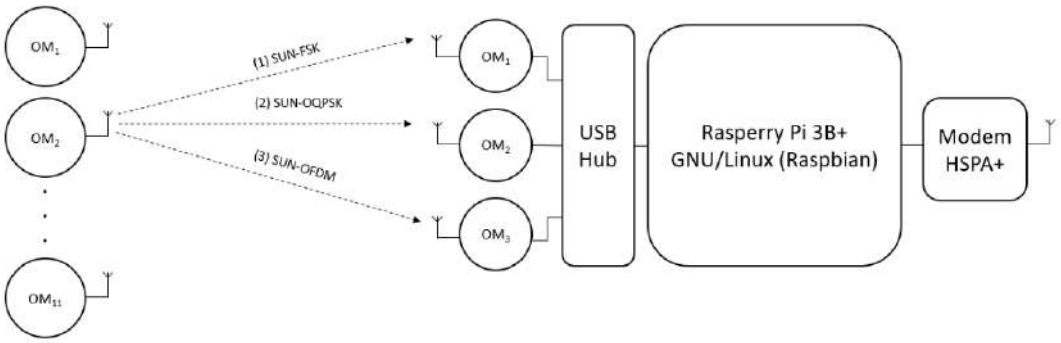

Figure 5.3: Hardware setup.

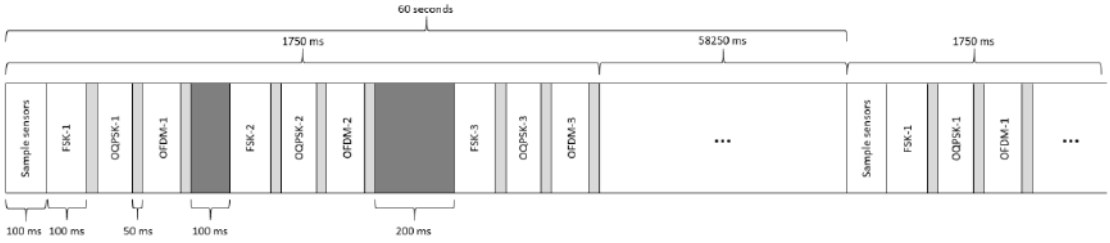

Figure 5.4: Transmission timeline.

the channel is considered safe to send the packet. The CCA threshold values for SUN-FSK, SUN-OQPSK and SUN-OFDM have been determined experimentally by the authors of [Tuset-Peiró et al., 2020c] and have been set to -94 dBm, -93 dBm and -91 dBm, respectively.

5.1.1 Sensors Clustering

Following the approach introduced in previous works on the same dataset [Gomes et al., 2020, Tuset-Peiró et al., 2020a], we have considered different groups of sensors based on their distance from the gateway and on their position in the warehouse where data has been collected. More specifically, nodes deployed within a distance of 80 m (56-53, 55-AD and 55-E4) have been included in the *close group*, nodes presenting a distance between 80m and 150m from the gateway (55-99, 55-DD, 55-65 and 56-0B) have been included in the *medium group* while all the remaining ones (56-32, 55-B3, 55-63 and 63-0A) have been considered as belonging to the *far group*.

Figure 5.5 represents the evolution of the ratio of received packages with respect

to the total transmission attempts number (PDR) for the defined sensor groups. The PDR variance is slightly reduced (in the plots the inter-quartile range is represented), especially in the *close group*. However it is evident from the plots how the group definition does not add enough information to easily predict the best SUN modulation given the previous history of the system. It is also worthy to notice how the quality of the channel is highly unstable sometimes dropping abruptly resulting in an average PDR value around 20%.

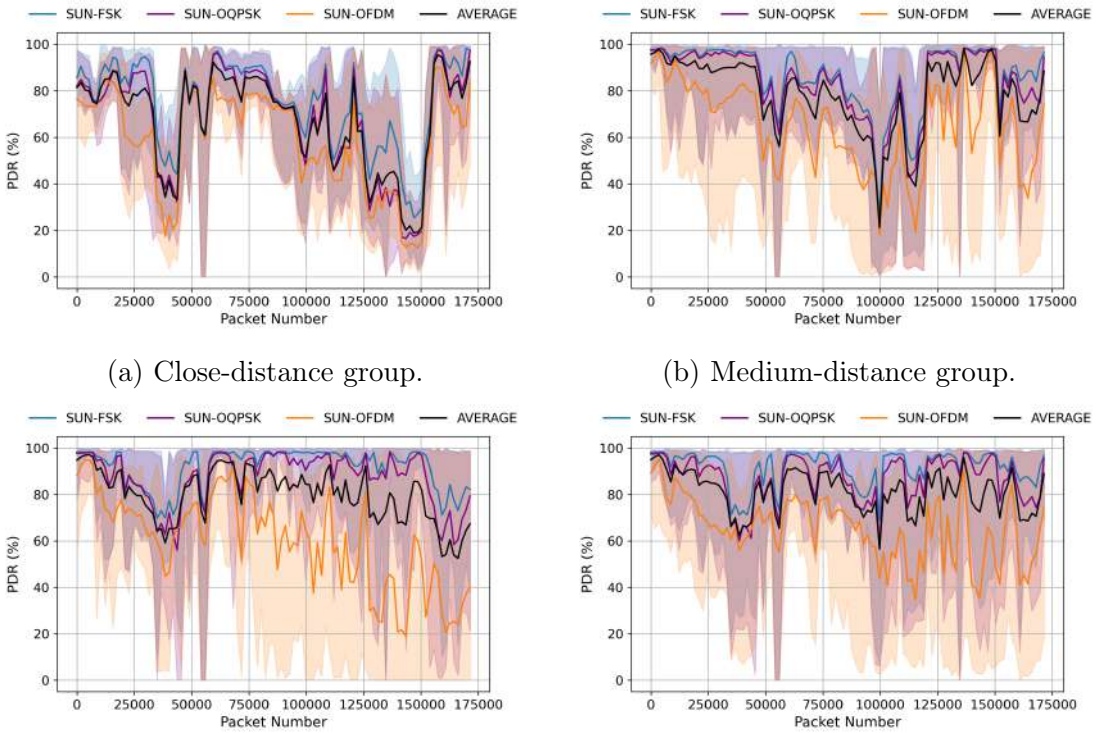

(a) Close-distance group.

(b) Medium-distance group.

(c) Far-distance group.

(d) All sensors.

Figure 5.5: Median (solid line) and inter-quartile range (shaded area) of the PDR for the SUN-FSK (blue), SUN-OQPSK (purple) and SUN-OFDM (orange) modulations, and the median computed over all modulations' PDR (solid black line) for different node groups. Median and inter-quartile range have been computed over PDR data stored in the trace file accumulated over one hour for all the devices in the data-set.

5.1.2 Trace Files

A *trace file* has been created from the original dataset estimating the transmission success probability for each modulation, by computing the frequency of successful transmissions over a sliding n minutes window ($n = 5$ was used in this analysis). The windows do not overlap: each new window starts where the previous one ends. To avoid windows with a transmitting probability equal to zero for all the modulations, windows have been spread until the first successful transmission has been found, the width of each window has been recorded. If no successful transmission has been recorded in more than 75 minutes, the corresponding window has been removed from the *trace file*. This was done to remove periods of time without packet reception due to the lack of Internet connection at the gateway, a problem known and described in the dataset specifics.

For each n-minutes wide window, n new packet transmission simulations have been run, where the probability of transmission corresponds to the frequency of successful transmissions within the window. Since in the real case a transmission attempt requires as much as 100ms and the time between two different packet transmissions is approximately one minute, all the re-transmissions of a specific packet has been ideally considered as instantaneous. As a consequence probability of transmission is considered to be equal for all the re-transmission attempts and there is no limit for the number of re-transmissions within a window.

From the sensor side, however, this is not sufficient to consider the transmission as successful. When the gateway receives the packets, transmits an ACK with the same modulation of the incoming packet. The probability of the ACK of being received is considered equal to the probability of transmitting the packet i.e. the channel is considered to be symmetric in the two directions of transmission. The sensor is able to detect a successful transmission only when the ACK is received.

5.2 Simulation process

To evaluate the modulation selection strategies a Python simulator has been deployed to simulate the transmission procedure and to implement the re-transmission shaping mechanism and the modulation selection strategies presented in the previous chapter as well as to compute the chosen evaluation parameters discussed in Section 5.2.1 and to simulate the other control strategies that are presented later in this Chapter in Section 5.2.2.

5.2.1 Evaluation parameters

As in [Gomes et al., 2020], the metrics that we are considering to evaluate the performances of the various solutions are the PDR (Packet Delivery Ratio), defined as the ratio between received and transmitted packets at the application layer, and the RNP (Required Number of Packet Transmissions), defined as the average number of packet repetitions before a successful transmission. We have computed those metrics after each attempt to transmit a distinct packet for each sensor and modulation selection strategy. Even though those metrics are related with each other, individually they are not sufficient to exhaustively describe the transmission properties. A low value of RNP (with respect to the maximum number of allowed re-transmissions) indicates that the packets are often received before the maximum number of re-transmission is reached. The RNP value, however, is upper bounded by the maximum number of allowed re-transmissions, therefore a high value of RNP may be associated with a low PDR if the re-transmission procedure stops because the maximum available number is reached or may be associated to a high PDR if the transmission succeeds frequently in correspondence to the last re-transmission. Consequently the PDR value is not useful to predict the RNP.

5.2.2 Modulation selection strategies

To implement the modulation selection strategies presented in Section 4.2 the simulator keeps in memory the set of the modulations as well as the estimated utility values of each modulation in order to select each time the most suited one. The maximum number of allowed re-transmission is given as input (it does not change as the re-transmission shaping mechanism is not implemented at this stage) and all the hyper-parameters needed by the various algorithms have been manually set. For each transmission attempt, the ACK is estimated by randomly sample it from a Bernoulli distribution presenting p equals to the transmission success probability obtained by the trace file. The ACK value is used to update the internal state of the modulation selector block by updating the utility score associated to each modulation. These updated values are used to select the subsequent modulation accordingly to the selected algorithm.

In addition, to provide a comparison term to the modulation selection strategies, the *RANDOM* and the *BEST* strategies have been implemented. The *RANDOM* strategy consists simply in randomly choosing a modulation for each transmission attempt from a uniform distribution. The *BEST* consists in choosing always the modulation associated with the highest probability of receiving the packet. Hence, the *RANDOM* strategy represents a lower performance bound, whereas the *BEST*

strategy represents an upper bound for the specific case.

In addition to the *RANDOM* and *BEST* strategies, we also compare the proposed modulation selection strategies to the *3M* strategy, which was introduced in [Gomes et al., 2020] and represents, to the best of our knowledge, the best result obtained so far to address the problem of dynamically select the best modulation in this specific scenario. In particular, for each transmission *3M* evaluates the probability to use of each modulation a according to

$$P_t(a) = \frac{(1 + ARR(a))^w}{\sum_{a' \in A}(1 + ARR(a'))^w}, \tag{5.1}$$

where parameter w is used to control the differences between the calculated probabilities and $ARR(a)$ is the *ACK Reception Ratio* defined as the ratio between the number of ACKs received successfully and the number of transmitted packets in a given interval with modulation a. The width of the interval used to compute $ARR(a)$ has been set equal to 10 consecutive re-transmissions while the value of w has been set equal to 20. Once $P_a(t)$ has been computed the algorithm then samples the modulation from the obtained probability distribution.

The parameters optimization process for the proposed algorithms should take into account the purpose of the methods, that should be able to adapt to a variety of environments. Because of that an offline tuning of hyperparameters on the basis of the knowledge of the channel evolution, by means of a grid search for example, is not to be taken in consideration since it would lead to a strong overfitting, invalidating the evaluation procedure.

The parameters used for the various algorithms are summarized in Table 5.2.

Algorithm	Parameters	
EG	$\alpha = 0.1$	$\tau = 0.1$
BE	$\alpha = 0.1$	$\epsilon = 0.1$
D-UCB	$\gamma = 0.9$	

Table 5.2: Parameters choice for the algorithms used.

An important aspect to validate the parameters choice is the results stability with respect to slight modification of the parameters themselves. This aspect has been investigated by running multiple transmission simulations with a reduced number of packets (1000) with different parameters choices and verifying that the performance remains almost invariant for moderate parameters variations.

A future development of this approach could consist in the on-line tuning of parameters, allowing the model to tune the balance between the exploration of the environment and the exploitation of results according to the stability of the channel performance.

5.2.3 Re-transmission Shaping

To simulate the transmission of a given data packet the simulator first determines the value of N_{ALLOWED} based on the values of N_{AVERAGE}, N_{MAXIMUM} and $N_{\text{AVAILABLE}}$ of the re-transmissions shaping mechanism, as described in Section 4.1. Then, for each N_{ALLOWED} the simulator determines which IEEE 802.15.4g SUN modulation to use using one of the two simple strategies available: *RANDOM* and *BEST*. In the *RANDOM* strategy the transmitting device randomly selects one of the three IEEE 802.15.4g SUN modulations available by sampling from a uniform distribution. In contrast, when using the *BEST* strategy the transmitting end-device always selects the modulation that has the best instantaneous PDR. Of course, the *BEST* strategy is an ideal scenario, as the instantaneous PDR value cannot be predicted in advance. However, using this strategy allows us to have an upper performance bound that allows to compare the performance of the *RANDOM* strategy too.

Once the modulation is selected, the channel simulator uses the PDR values for the given IEEE 802.15.4g SUN modulation and end-device, which have been obtained from the data-set, to determine if a the data packet transmission and its acknowledgment are successfully received or not. It does so by comparing a randomly generated number using a uniform distribution with the computed PDR value for the current data packet transmission. If the random value is below the computed PDR value the data packet is considered as successfully received. Otherwise, the data packet is considered as not successfully received. If the data packet is successfully received, the process is then repeated for the acknowledgment packet using the same PDR value and procedure. That is, the simulator assumes that links are symmetric and data packets are received according to a Bernoulli trial with probability equal to the computed PDR value.

The process is repeated until the data packet and the acknowledgment are successfully received or the number of transmissions for the current data packet reaches N_{ALLOWED}. If the data packet and the acknowledgment are successfully received, the channel simulator returns the number of transmissions used (N_{USED}) for the current packet to the re-transmission shaping module. On the contrary, if the data packet has not been successfully received the simulator returns 0 to the re-transmission shaping module, indicating that all transmission attempts have been used.

Finally, upon receiving N_{USED} value the re-transmission shaping mechanism updates the $N_{\text{AVAILABLE}}$ value according to Equation 4.2 and the process is repeated for the remaining data packet transmissions.

5.2.4 Combined Methods

As explained in Section 4.3 the re-transmission shaping and the modulation selector blocks operate almost independently so it is straightforward to implement them in conjunction. The value of $\text{N}_{\text{ALLOWED}}$ outputted by the re-transmission shaping module is received as input by the modulation selector module, determining the required value of $\text{N}_{\text{MAXIMUM}}$ for each packet. The modulation selector module instead needs to be slightly modified by keeping in memory the number of re-transmission used for each packet N_{USED}. Once the allowed number of re-transmissions is completed or the ACK is received, the modulation selector module sends the value of N_{USED} to the re-transmission shaping module that uses this value to update the internal variable $\text{N}_{\text{AVAILABLE}}$ accordingly to Equation 4.2.

Chapter 6

Results

This section presents the results obtained when applying the dynamic modulation selection strategies and re-transmission shaping to the IEEE 802.15.4g SUN dataset presented in Section 5.1 with the objective of improving link reliability. In particular, Section 6.1 presents the results for modulation selection, Section 6.2 presents the results for re-transmission shaping and, finally, Section 6.3 presents the results for combining modulation selection with re-transmission shaping.

In all cases the PDR and RNP metrics have been used to evaluate results and the results presented are the average for 30 repetitions for each maximum number of packet re-transmissions value. This has be done in order to reduce the variability of the simulations thus increasing the consistency of results.

In all the plots showing the evolution of some metric through time, it is important to notice that the x-axis represents the number of different packets sent. Since the re-transmission procedure has been approximated as instantaneous, the lines shown in each plot are synchronized in time, making it possible to observe the common behaviour of the series in correspondence of a drop in the channel reliability caused by environmental conditions.

6.1 Modulation selection

Figures 6.1 and 6.2 presents the evolution of the average PDR and the RNP respectively for 3 re-transmissions per packet (i.e., RTX=3), whereas Table 6.1 presents the raw values for a different number of packet re-transmissions (i.e., RTX=1, 2, 3, 6 and 9, respectively).

Regarding the two Figures, it can be remarked the following:

- the drops in the PDR and the corresponding boosts in RNP are caused by a drop in the quality of all the available channels, as can noticed by the fact that the *BEST* strategy follows the same general schema of the other modulation selection strategies;
- even though the metrics values can vary during the various transmission attempts, the relative order of the best performing strategies remains invariant;
- as expected, the *BEST* and *RANDOM* strategies present respectively the highest and lowest PDR and the lowest and the highest RNP for all the groups and for each number of packet transmissions;
- none of the strategies, including *BEST*, is able to reach PDR values close to 99%.

For what concerns the role of the modulation selection strategies to improve the *RANDOM* re-transmission strategy, we can notice how all the proposed strategies perform similarly and are also close to the *3M* strategy as shown in Table 6.1. The gap between the best performing strategy between the non trivial ones (EG) and the worst one (3M) is noticeable, being close to one percentage point. In the global scenario (All-distance group) the *EG* strategy allows us to increase the base PDR (with *RANDOM* strategy) by two percentage points (from 94% to 96%) while also decreasing the RNP from 1.48 to 1.32, resulting in an overall more efficient transmission strategy.

Figure 6.3 presents the variation of the final PDR-RNP values by varying the maximum number of allowed re-transmissions (RTX) for the different groups. The values used to explore different performances are 1, 2, 3, 6, 9. This range of values is wide enough to observe different relative variation of metrics within the explored modulation selection strategies: for RTX=1 the value of RNP is trivially equal for all the strategies while the PDR difference is maximum. Increasing the RTX value the PDR difference is reduced while the RNP difference increases, when RTX is equal to 9 the PDR difference is almost negligible while the RNP is widely spread going from 1.55 for the *BEST* strategy to 1.97 for the *RANDOM* strategy with a relative increase of 27%. As depicted in Figure 6.3, we observe that the *BE* and *EG* provide a PDR=0.95 with a RNP=1.35 for 3 re-transmissions. In contrast, the *3M* strategy provide an average PDR=0.90 and a RNP=1.21 for the same number of re-transmissions. This represents an increase of 5.3% in the PDR and a reduction of RNP of 10.4%.

The role of the modulation selections is particularly evident in the case of one transmission per packet. The EG strategy is able to bring the PDR from the baseline

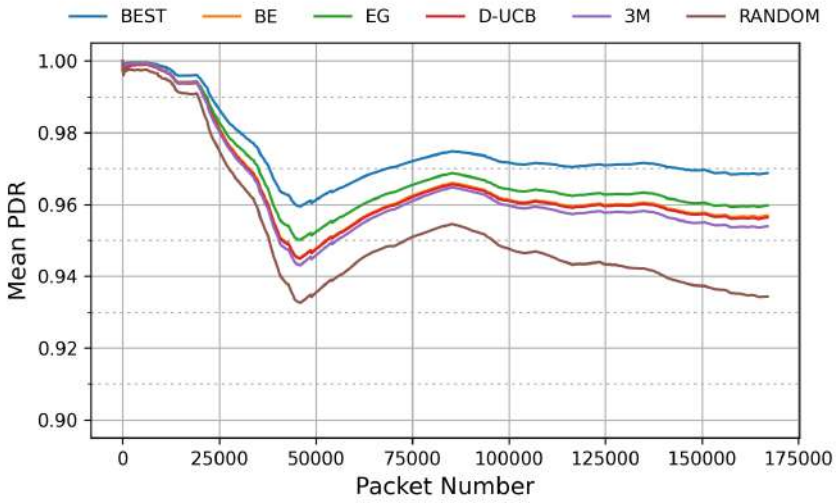

Figure 6.1: Temporal evolution of accumulated PDR for all the modulation selection strategies averaged for different node groups with $N_{\mathrm{AVG}} = 3$ re-transmissions per packet.

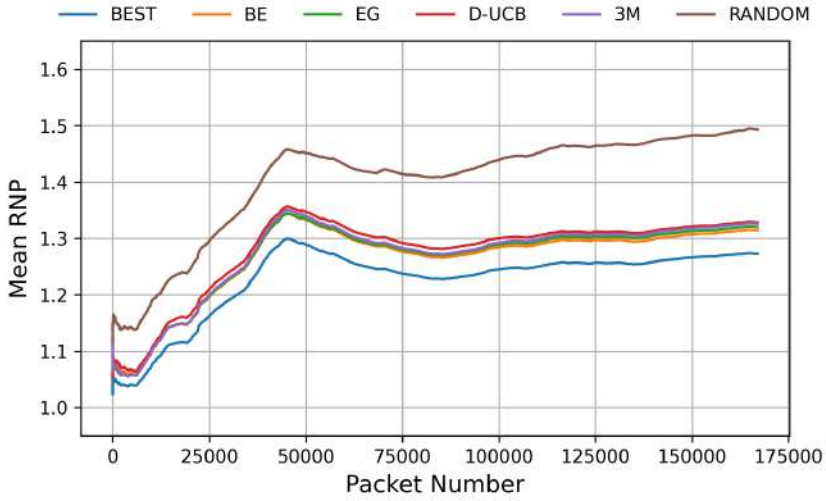

Figure 6.2: Temporal evolution of accumulated RNP for all the modulation selection strategies averaged for different node groups with $N_{\mathrm{AVG}} = 3$ re-transmissions per packet.

of 78% (*RANDOM* strategy) to 86% with no increase in the RNP, performing almost midway between *3M* (82%) and *BEST* (89%).

On the other extreme, with the highest explored number of re-transmissions ($N_{\text{AVG}} = 9$) the differences between PDR values weakens (99% for the *BEST* against 98% for the *RANDOM* strategy) but *EG* strategy actually needs 15% less re-transmissions than *RANDOM* (1.66 against 1.95).

Overall, this shows the possibility for the proposed modulation selection strategies to obtain higher performances in one of the two metrics at the cost of performing worse in the other one. The optimal threshold to mediate between the necessity of keeping the number of transmission low while loosing the lowest information possible can be evaluated according to the specific implementation requirements.

It should be remarked how the evolution of the metrics for maximum re-transmission values different then 3 are similar to what shown in Figures 6.1 and 6.2 with the relative order of the best performing modulation selection strategies remaining invariant and a trend similar to the case of RTX=3 with higher PDR as RTX increases and higher RNP as RTX decreases, as explained before.

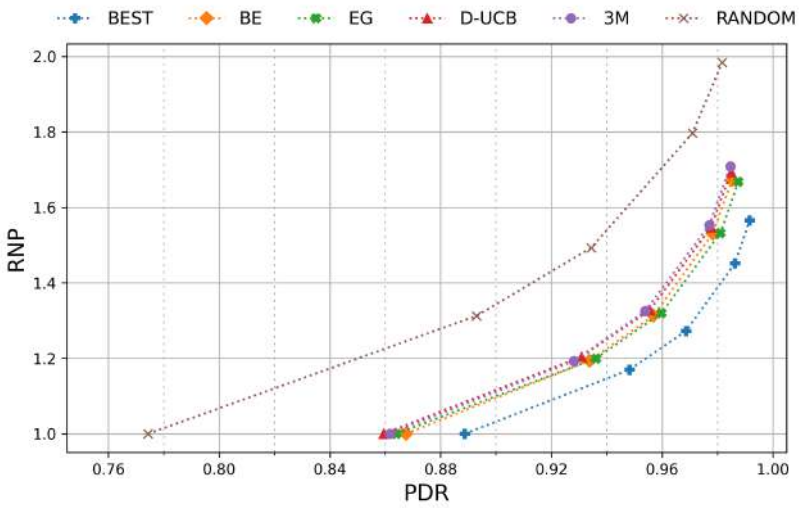

Figure 6.3: Final PDR-RNP values for different maximum re-transmission values (i.e., 1, 2, 3, 6 and 9) for all the discussed modulation selection strategies and for all nodes groups.

Group	Strat	$N_{\text{AVG}} = 1$		$N_{\text{AVG}} = 2$		$N_{\text{AVG}} = 3$		$N_{\text{AVG}} = 6$		$N_{\text{AVG}} = 9$	
		PDR	RNP	PDR	RNP	PDR	RNP	PDR	RNP	PDR	RNP
Close	*RND*	75%	1.00	88%	1.37	93%	1.59	98%	1.95	99%	2.16
	3M	82%	1.00	92%	1.25	95%	1.43	98%	1.70	99%	1.86
	EG	83%	1.00	93%	1.26	96%	1.41	99%	1.66	99%	1.79
	BST	86%	1.00	94%	1.22	97%	1.34	99%	1.54	100%	1.64
Med	*RND*	78%	1.00	89%	1.30	93%	1.49	96%	1.84	97%	2.07
	3M	85%	1.00	91%	1.21	94%	1.36	97%	1.64	98%	1.85
	EG	85%	1.00	92%	1.21	95%	1.35	97%	1.62	98%	1.80
	BST	87%	1.00	93%	1.19	96%	1.31	98%	1.54	99%	1.70
Far	*RND*	79%	1.00	90%	1.28	94%	1.42	98%	1.64	98%	1.77
	3M	91%	1.00	95%	1.13	97%	1.22	98%	1.36	99%	1.46
	EG	90%	1.00	96%	1.14	97%	1.22	99%	1.35	99%	1.44
	BST	93%	1.00	97%	1.11	98%	1.18	99%	1.30	99%	1.37
All	*RND*	77%	1.00	89%	1.31	93%	1.49	97%	1.80	98%	1.98
	3M	86%	1.00	93%	1.19	95%	1.33	98%	1.55	98%	1.71
	EG	86%	1.00	94%	1.20	96%	1.32	98%	1.53	99%	1.67
	BST	89%	1.00	95%	1.17	97%	1.27	99%	1.45	99%	1.56

Table 6.1: Final PDR-RNP values for different maximum re-transmission values (1, 2, 3, 6, 9) and without re-transmission shaping for *RANDOM*, *3M*, *EG* and *BEST* modulation selection strategies for all nodes groups.

6.2 Re-transmission shaping

In this subsection it will be analyzed the benefits of adding re-transmission shaping, which allows to accumulate the unused packet re-transmissions and use them at a later moment to compensate for the lower PDR values that may occur unexpectedly due to propagation and interference conditions.

Figures 6.7 and 6.7 respectively present the evolution of the PDR and RNP metrics for the *RANDOM* and *BEST* strategies with and without re-transmission shaping for $N_{\text{AVERAGE}} = 3$. The results are the average of all the devices present in the deployment.

As it can be observed, re-transmission shaping allows to increase the PDR for both the *RANDOM* and the *BEST* strategies. In particular, re-transmission shaping increases the PDR by 4.92% (from 0.935 to 0.981) for the *RANDOM* strategy and by

2.17% (from 0.969 to 0.990) for the *BEST* strategy. Regarding RNP, re-transmission shaping increases the average RNP for both the *RANDOM* and the *BEST* strategies. Specifically, re-transmission shaping increases the RNP by 40% (from 1.50 to 2.10) for the *RANDOM* strategy and by 27% (from 1.26 to 1.6) for the *BEST* strategy.

In turn, Figure 6.6 and Table 6.2 show the relation between the PDR and the RNP metrics for different values of average re-transmissions per packet (i.e., $N_{\text{AVG}} = \{2, 3, 6, 9\}$) and maximum re-transmissions per packet (i.e., $N_{\text{MAXIMUM}} = 9$). For $N_{\text{AVERAGE}} = 1$ we can observe that PDR is 77.4% and 88.9% for the *BEST* and *RANDOM* strategies regardless of whether re-transmission shaping is enabled or not. Also, for $N_{\text{AVERAGE}} = 1$ we have that $RNP = 1$ for all cases. Both results are expected, as we only allow one packet re-transmission per packet and, hence, the re-transmission shaping does not make any effect.

It is interesting to notice that for the *RANDOM* strategy with $N_{\text{AVERAGE}} = 2$ using re-transmission shaping the PDR improves by 6.9% (from 89.3% to 96.2%) while the RNP increases 35.9% (from 1.31 to 1.78). In contrast, adding another transmission attempt to the *RANDOM* strategy without re-transmission shaping would increase PDR by 4.6% (from 89.3% to 93.4%) while the RNP would increase by 13.7% (from 1.31 to 1.49). Of course, increasing the PDR is more difficult as its value approaches 100%, but the mean RNP value is still below the target (i.e., $N_{\text{AVERAGE}} = 2$). Adding more re-transmissions per packet allows to further increase the PDR at the expense of increasing the RNP and, hence, the energy consumption. With $N_{\text{AVERAGE}} = 6$ and re-transmission shaping the PDR reaches 98.8%, whereas with $N_{\text{AVERAGE}} = 9$ the PDR reaches 99.2%. Of course, the RNP raises to 2.20 and 2.35 respectively, indicating that more packets are required on average.

		$N_{\text{AVG}} = 1$		$N_{\text{AVG}} = 2$		$N_{\text{AVG}} = 3$		$N_{\text{AVG}} = 6$		$N_{\text{AVG}} = 9$	
RS	Strat	PDR	RNP	PDR	RNP	PDR	RNP	PDR	RNP	PDR	RNP
No	*RND*	77.4%	1.00	89.3%	1.31	93.4%	1.49	97.1%	1.80	98.2%	1.98
	BST	88.9%	1.00	94.8%	1.17	96.9%	1.27	98.6%	1.45	99.2%	1.56
Yes	*RND*	77.4%	1.00	96.2%	1.78	98.2%	2.03	98.8%	2.20	99.2%	2.35
	BST	88.9%	1.00	98.5%	1.51	99.1%	1.59	99.5%	1.72	99.6%	1.79

Table 6.2: Final PDR-RNP values for the *RANDOM* and *BEST* modulation selection strategies with and without the re-transmission shaping (RS) mechanism for $N_{\text{AVERAGE}} = \{2, 3, 6, 9\}$ and $N_{\text{MAXIMUM}} = 9$.

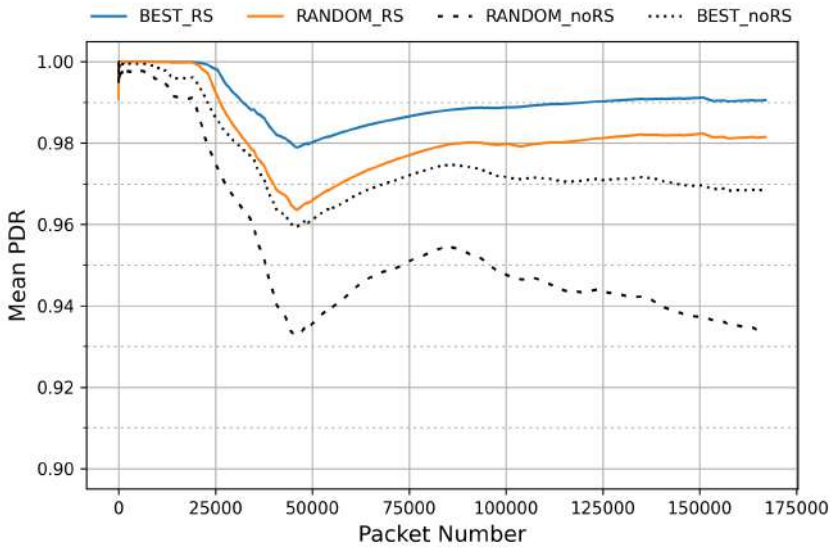

Figure 6.4: Temporal evolution of accumulated PDR (a) and RNP (b) values for the *RANDOM* and *BEST* strategies with and without re-transmission shaping using $N_{\text{AVERAGE}} = 3$ re-transmissions per data packet.

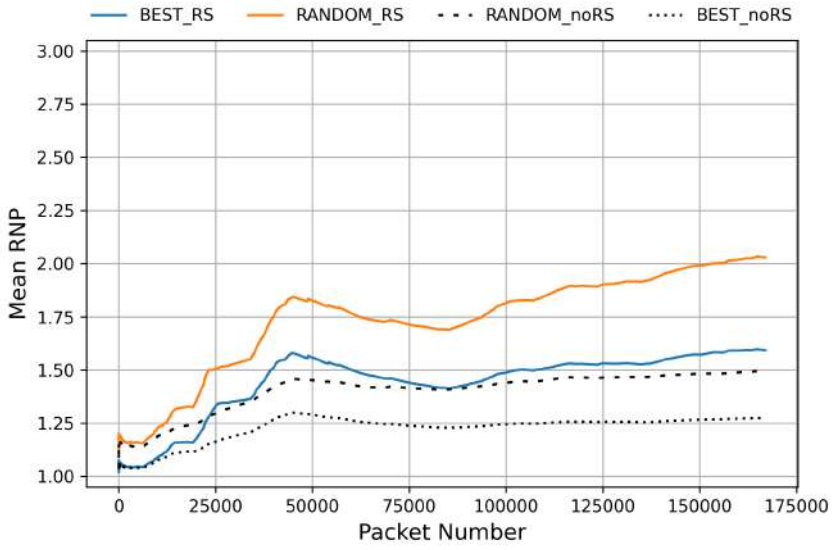

Figure 6.5: Temporal evolution of accumulated PDR (a) and RNP (b) values for the *RANDOM* and *BEST* strategies with and without re-transmission shaping using $N_{\text{AVERAGE}} = 3$ re-transmissions per data packet.

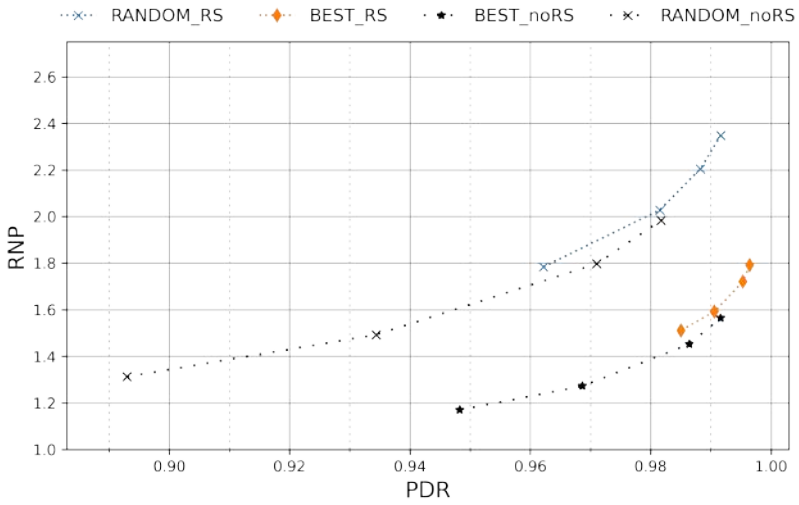

Figure 6.6: Final PDR-RNP values for the *RANDOM* and *BEST* re-transmission strategies with and without the re-transmission shaping mechanism. The results are presented for $N_{\text{AVERAGE}} = \{2, 3, 6, 9\}$ and $N_{\text{MAXIMUM}} = 9$.

6.3 Combined Results

In this subsection are explored the benefits brought by combining the modulation selection strategies, whose individual effect has been presented in Section 6.1, and with the energy shaping, whose individual effect has been presented in Section 6.2.

A more efficient allocation of the available energy can drastically improve the PDR values while keeping the RNP under a specified threshold; combining this with an optimized selection of the modulation used to send each packet leads to a nearly optimal transmission schedule, given the constraints of the available power and the channel impairments.

In Figure 6.7 and 6.8 the accumulated PDR and RNP are plotted against the number of packets transmission attempts, as discussed for Figure 6.1 and 6.2. For seek of easy of read, only the *all-distances group* results have been graphically shown in this chapter. The plots related to all the other groups have been inserted in Appendix for easy of read. For the *all-distances group* the *RANDOM* strategy with energy shaping presents higher PDR than the *BEST* strategy in the base case. For all the groups the improvement in PDR due to the application of the modulation selection strategies over what can be achieved with the 3M strategy is within one percentage point. The gap between the *RANDOM* and *BEST* strategies however is strongly

reduced respect to the case in which only the modulation selection has been applied, being always below four percentage points.

With a specific focus to the *RANDOM-BEST* gap, indeed, it is worthy to remark how the modulation selection strategies is able to reduce the PDR gap up to 61% (with *EG* algorithm) against 27% obtained with *3M* algorithm with energy shaping with 3 re-transmissions per packet averaged over all distance nodes. This effect is shown in the side box of Figure 6.7. The reduction in RNP is slighter but still noticeable since the *EG* algorithm reduces the RNP gap of 76% against the 65% obtained by 3M as shown in the side box of Figure 6.8.

In Figure 6.7 we have to comment that all reinforced learning strategies perform similar in terms of PDR and RNP, with the EG strategy performing slightly better for the *medium-distance group*. This can be expected, as in the *medium-distance group* the delivery probabilities for the different modulations are similar and, hence, it is more difficult to learn which to use.

As in previous cases, it can be noticed that in Figure 6.8 there is a sharp rise in the mean RNP around packet 25000 and it is flat afterwards. This sharp rise is because the PDR is bad and we have to spend the energy surplus accumulated from past transmissions to compensate. The flat area is because the PDR is still bad but we do not have more packets than the average. After the PDR becomes better we begin to save energy again, which can be used later to compensate.

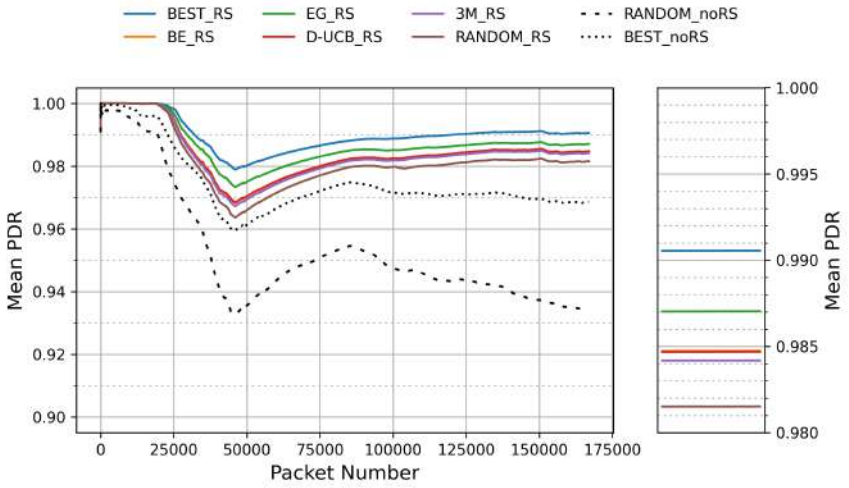

Figure 6.7: Temporal evolution of accumulated PDR for all the modulation selection strategies with energy shaping for all distance nodes with 3 re-transmissions per packet. Baseline tracks for *RANDOM* and *BEST* strategies without energy shaping for the same re-transmission value are included for comparison. The side box shows in greater scale the final PDR values for all the tracks except for the baselines.

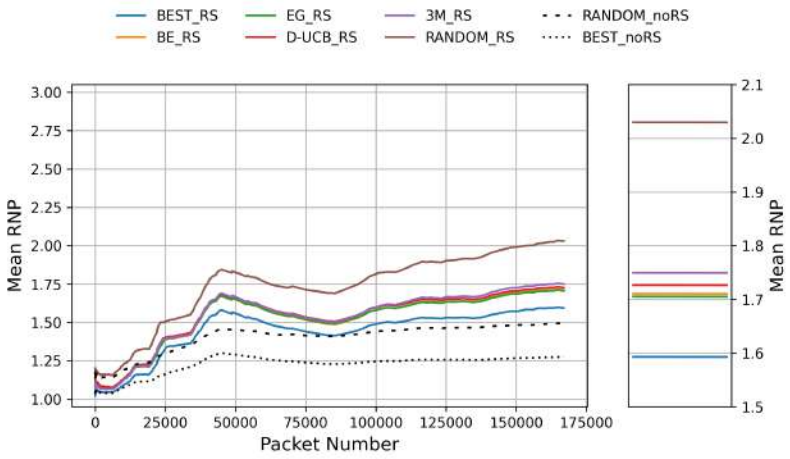

Figure 6.8: Temporal evolution of accumulated RNP for all the modulation selection strategies with energy shaping for all distance nodes with 3 re-transmissions per packet. Baseline tracks for *RANDOM* and *BEST* strategies without energy shaping for the same re-transmission value are included for comparison. The side box shows in greater scale the final RNP values for all the tracks except for the baselines.

Group	Strat	$N_{\text{AVG}} = 2$		$N_{\text{AVG}} = 3$		$N_{\text{AVG}} = 6$		$N_{\text{AVG}} = 9$	
		PDR	RNP	PDR	RNP	PDR	RNP	PDR	RNP
Close	*RND*	96%	1.92	99%	2.30	100%	2.40	100%	2.49
	3M	99%	1.84	99%	1.97	100%	2.05	100%	2.12
	EG	99%	1.81	100%	1.89	100%	1.96	100%	2.01
	BST	100%	1.69	100%	1.71	100%	1.76	100%	1.80
Med	*RND*	95%	1.76	97%	2.00	98%	2.31	99%	2.58
	3M	96%	1.59	97%	1.80	98%	2.08	99%	2.31
	EG	96%	1.57	98%	1.76	99%	2.04	99%	2.20
	BST	97%	1.51	98%	1.66	99%	1.92	100%	2.04
Far	*RND*	98%	1.71	99%	1.86	99%	1.95	99%	2.02
	3M	99%	1.46	99%	1.53	99%	1.60	99%	1.67
	EG	99%	1.44	99%	1.51	99%	1.57	99%	1.63
	BST	99%	1.38	99%	1.43	99%	1.48	100%	1.53
All	*RND*	96%	1.78	98%	2.03	99%	2.20	99%	2.35
	3M	97%	1.61	98%	1.75	99%	1.90	99%	2.02
	EG	98%	1.59	99%	1.70	99%	1.85	99%	1.94
	BST	99%	1.51	99%	1.59	100%	1.72	100%	1.79

Table 6.3: Final PDR-RNP values for the *RANDOM*, *3M*, *EG* and *BEST* modulation selection strategies with Energy Shaping. The results are presented for $N_{\text{AVG}} = \{2, 3, 6, 9\}$ and $N_{\text{MAX\_SURPLUS}} = 12$ for all nodes groups (i.e., close, medium, far and all).

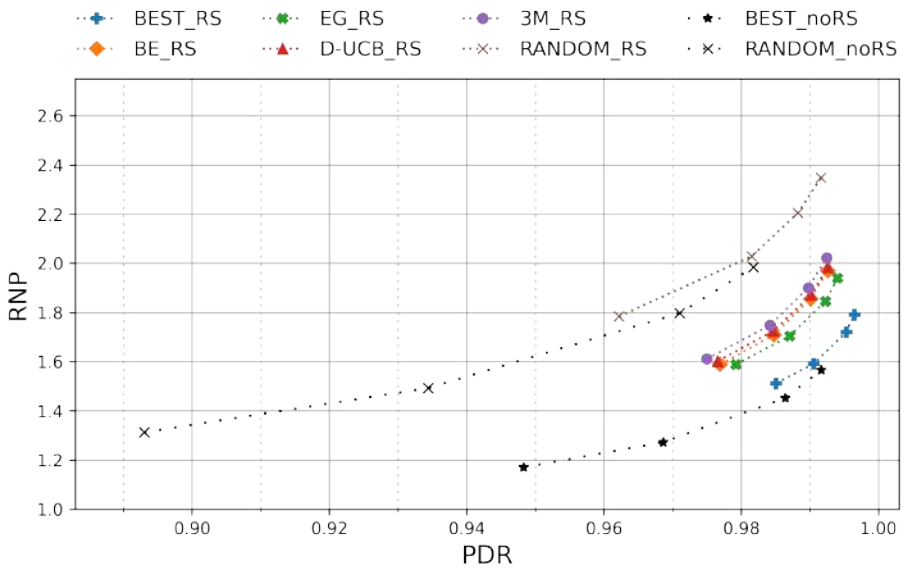

Figure 6.9: Final PDR-RNP values for different values of average re-transmission numbers (i.e., 2, 3, 6 and 9 re-transmissions per packet and $N_{\text{MAX\_SURPLUS}}$=9) for all the modulation selection strategies with energy shaping for all distance nodes. Baseline tracks for *RANDOM* and *BEST* strategies without energy shaping for the same set of re-transmission values are included for comparison.

Chapter 7

Conclusions and Future Work

7.1 Conclusions

This thesis work has introduced the application of dynamic modulation selection in the context of IEEE 802.15g SUN alongside a novel mechanism of redistribution of available transmission power. These two mechanisms aim to improve the communication reliability of IEEE 802.15g SUN (Smart Utility Networks), a communication standard of extreme interest in the IoT (Internet of Things) area.

Regarding energy shaping, we have designed a simple algorithm that takes two input values describing the average number of available re-transmissions per packet (N_{AVERAGE}) and the maximum number of extra re-transmissions allowed for any single packet ($N_{\text{MAX\_SURPLUS}}$). Based on these two values, the algorithm chooses each time the maximum number of re-transmission allowed for the current packet (N_{ALLOWED}). With respect to the standard re-transmission approach, consisting in re-transmitting the packet up to a fixed maximum allowed re-transmission value, our method shows higher percentage of delivered packets while enforcing the energy constraints. Another advantage consists in the fact that N_{AVERAGE} is not required to be an integer, allowing for a finer tuning of the energy requirements.

Regarding the dynamic modulation selection strategies, various MAB (Multi-Armed Bandit) algorithms have been applied to determining the best combination of IEEE 802.15.4g SUN modulations (i.e., FSK, OQPSK and OFDM) to transmit a given number of packet repetitions (i.e., 1, 2, 3, 6 and 9, respectively).

To evaluate their performance, both strategies have been applied to a dataset obtained from a real-world scenario and we have used the PDR (Packet Delivery Ratio) and the RNP (Required Number of Packets) as the metrics to determine the suitability of each approach.

The results show that both modulation selection and energy shaping are useful tools to improve link quality of IEEE 802.15.4g SUN networks. Each strategy alone allows to improve over the baseline and, as expected, combining them allows to achieve the best results. The re-transmission shaping improves the distribution of the available energy, determining an efficient choice of the maximum number of re-transmissions per packet. The modulation selection, complementary, works considering the number of available transmissions per packet as assigned. It aims to determine for each transmission attempts the channel with the highest success probability. This allows to significantly reduce the performance gap between the already existing modulation selection algorithms [Tuset-Peiró et al., 2020b] and the theoretically best possible strategy. The joint use of the two methods is capable of meeting the industrial requirements specific for this application (i.e., 99% of PDR) with a RNP value of 1.7.

Hence, we conclude that applying adaptive modulation selection and energy shaping is a good to improve reliability of IEEE 802.15.4g SUN deployments.

7.2 Future Work

Given the interest of the results and its potential applicability to a real-world environment, as future work we will implement the different modulation selection algorithms in a real-world scenario to validate that the findings are applicable considering the impact on node energy consumption. The obtained savings in terms of re-transmissions are worthless if the computational cost of the algorithms used to achieve this goal requires an energy expenditure higher than the energy saved by reducing the number of transmissions.

Another relevant aspect to investigate is the optimal value of N_{MAXIMUM} as a function of other parameters stored in the re-transmission module to optimize performances of re-transmission shaping. For example, it is possible to hypothesize that reducing the value of N_{MAXIMUM} in correspondence of a low value of $N_{\text{AVAILABLE}}$ (i.e., when the average energy consumption is close to its maximum allowed value) could help improving performances.

Bibliography

[A. Mulligan and Olsson, 2013] A. Mulligan, C. E. and Olsson, M. (2013). Architectural implications of smart city business models: an evolutionary perspective. *IEEE Communications Magazine*, 51(6):80–85.

[Bombino et al., 2020] Bombino, A., Grimaldi, S., Mahmood, A., and Gidlund, M. (2020). Machine learning-aided classification of los/nlos radio links in industrial iot. In *IEEE WFCS 2020*.

[Castellani et al., 2011] Castellani, A. P., Gheda, M., Bui, N., Rossi, M., and Zorzi, M. (2011). Web services for the internet of things through coap and exi. In *2011 IEEE International Conference on Communications Workshops (ICC)*, pages 1–6.

[Cesa-Bianchi et al., 2017] Cesa-Bianchi, N., Gentile, C., Lugosi, G., and Neu, G. (2017). Boltzmann exploration done right.

[Chauvet et al., 2019] Chauvet, N., Jegouso, D., Boulanger, B., Saigo, H., Okamura, K., Hori, H., Aurelien, D., Huant, S., Bachelier, G., and Naruse, M. (2019). Entangled-photon decision maker. *Scientific Reports*, 9:12229.

[CISCO, 2010] CISCO (2010). Evaluating interference in wireless lans: Recommended practice.

[Dakdouk et al., 2018] Dakdouk, H., Tarazona, E., Alami, R., Féraud, R., Papadopoulos, G. Z., and Maillé, P. (2018). Reinforcement learning techniques for optimized channel hopping in ieee 802.15.4-tsch networks. In *Proceedings of the 21st ACM International Conference on Modeling, Analysis and Simulation of Wireless and Mobile Systems*, MSWIM '18, page 99–107, New York, NY, USA. Association for Computing Machinery.

[Gomes et al., 2018] Gomes, P. H., Watteyne, T., and Krishnamachari, B. (2018). Mabo-tsch: Multihop and blacklist-based optimized time synchronized channel

hopping. *Transactions on Emerging Telecommunications Technologies*, 29(7):e3223. e3223 ett.3223.

[Gomes et al., 2020] Gomes, R., Tuset-Peiro, P., and Vilajosana, X. (2020). Improving link reliability of ieee 802.15.4g sun networks with adaptive modulation diversity.

[Gomes et al., 2019] Gomes, R. D., Benavente-Peces, C., Fonseca, I. E., and Alencar, M. S. (2019). Adaptive and beacon-based multi-channel protocol for industrial wireless sensor networks. *Journal of Network and Computer Applications*, 132:22 – 39.

[Gubbi et al., 2013] Gubbi, J., Buyya, R., Marusic, S., and Palaniswami, M. (2013). Internet of things (iot): A vision, architectural elements, and future directions. *Future Generation Computer Systems*, 29(7):1645 – 1660. Including Special sections: Cyber-enabled Distributed Computing for Ubiquitous Cloud and Network Services & Cloud Computing and Scientific Applications — Big Data, Scalable Analytics, and Beyond.

[Hartland et al., 2011] Hartland, C., Baskiotis, N., Gelly, S., Sebag, M., and Teytaud, O. (2011). Change point detection and meta-bandits for online learning in dynamic environments.

[Hasegawa et al., 2020] Hasegawa, S., Kim, S., Shoji, Y., and Hasegawa, M. (2020). Performance evaluation of machine learning based channel selection algorithm implemented on iot sensor devices in coexisting iot networks. In *2020 IEEE 17th Annual Consumer Communications Networking Conference (CCNC)*, pages 1–5.

[IEEE, 2012] IEEE (2012). Ieee standard for local and metropolitan area networks–part 15.4: Low-rate wireless personal area networks (lr-wpans) amendment 1: Mac sublayer. *IEEE Std 802.15.4e-2012 (Amendment to IEEE Std 802.15.4-2011)*, pages 1–225.

[Kim and Aono, 2015] Kim, S.-J. and Aono, M. (2015). Decision maker using coupled incompressible-fluid cylinders.

[Lai and Robbins, 1985] Lai, T. and Robbins, H. (1985). Asymptotically efficient adaptive allocation rules. *Advances in Applied Mathematics*, 6(1):4 – 22.

[Muñoz et al., 2018] Muñoz, J., Chang, T., Vilajosana, X., and Watteyne, T. (2018). Evaluation of ieee802.15.4g for environmental observations. *Sensors*, 18(10).

[Muñoz et al., 2018a] Muñoz, J., Muhlethaler, P., Vilajosana, X., and Watteyne, T. (2018a). Why channel hopping makes sense, even with ieee802.15.4 ofdm at 2.4 ghz. In *2018 Global Internet of Things Summit (GIoTS)*, pages 1–7.

[Muñoz et al., 2018b] Muñoz, J., Riou, E., Vilajosana, X., Muhlethaler, P., and Watteyne, T. (2018b). Overview of ieee802.15.4g ofdm and its applicability to smart building applications. In *2018 Wireless Days (WD)*, pages 123–130.

[Park et al., 2010] Park, P., Fischione, C., and Johansson, K. H. (2010). Adaptive IEEE 802.15.4 Protocol for Energy Efficient, Reliable and Timely Communications. In *Proceedings of the 9th ACM/IEEE International Conference on Information Processing in Sensor Networks*, IPSN '10, page 327–338, New York, NY, USA. Association for Computing Machinery.

[Savazzi et al., 2019] Savazzi, P., Goldoni, E., Vizziello, A., Favalli, L., and Gamba, P. (2019). A wiener-based rssi localization algorithm exploiting modulation diversity in lora networks. *IEEE Sensors Journal*, 19(24):12381–12388.

[Solimini et al., 2020] Solimini, D., Tuset-Peiró, P., Boquet, G., Vilajosana, X., and Vázquez-Gallego, F. (2020). Improving link reliability of ieee 802.15.4g sun with re-transmission shaping. *17th ACM Symposium on Performance Evaluation of Wireless Ad Hoc, Sensor, & Ubiquitous Networks(PE-WASUN'20)*.

[Solimini et al., 2021] Solimini, D., Tuset-Peiró, P., Gomez, R. D., Vilajosana, X., and Vázquez-Gallego, F. (2021?). Towards reliable ieee 802.15.4g sun with adaptive modulation selection and energy shaping. *Manuscript in preparation*.

[Sousa et al., 2014] Sousa, M. P., Lopes, W. T. A., Madeiro, F., and Alencar, M. S. (2014). Cooperative modulation diversity applied to heterogeneous wireless sensor networks. In *2014 IEEE International Conference on Distributed Computing in Sensor Systems*, pages 338–343.

[Sutton and Barto, 2018] Sutton, R. S. and Barto, A. G. (2018). *Reinforcement Learning: An Introduction*. A Bradford Book, Cambridge, MA, USA.

[Taheri Javan et al., 2020] Taheri Javan, N., Sabaei, M., and Hakami, V. (2020). Ieee 802.15.4.e tsch-based scheduling for throughput optimization: A combinatorial multi-armed bandit approach. *IEEE Sensors Journal*, 20(1):525–537.

[Takeuchi et al., 2020] Takeuchi, S., Hasegawa, M., Kanno, K., Uchida, A., Chauvet, N., and Naruse, M. (2020). Dynamic channel selection in wireless communications

via a multi-armed bandit algorithm using laser chaos time series. *Scientific Reports*, 10:1574.

[Turkka and Renfors, 2008] Turkka, J. and Renfors, M. (2008). Path loss measurements for a non-line-of-sight mobile-to-mobile environment. In *ITS Telecommunications, 2008. ITST 2008. 8th International Conference on*, pages 274 – 278.

[Tuset-Peiro et al., 2013] Tuset-Peiro, P., Adelantado, F., Vilajosana, X., Vázquez-Gallego, F., and Alonso-Zarate, J. (2013). On the use of the 433 mhz band to improve the energy efficiency of m2m communications. In *Personal Indoor and Mobile Radio Communications (PIMRC), 2013 IEEE 24th International Symposium onAt: London, United KingdomVolume: 2013*.

[Tuset-Peiró et al., 2020a] Tuset-Peiró, P., Adelantado, F., Vilajosana, X., and Gomes, R. (2020a). Improving Reliability With Modulation Diversity for IEEE 802.15.4g Smart Utility Networks. In *2020 IEEE Symposium on Computers and Communications (ISCC)*.

[Tuset-Peiró et al., 2020b] Tuset-Peiró, P., Adelantado, F., Vilajosana, X., and Gomes, R. (2020b). Reliability through modulation diversity: can combining multiple IEEE 802.15.4-2015 SUN modulations improve PDR? In *2020 IEEE Symposium on Computers and Communications (ISCC)*.

[Tuset-Peiró et al., 2020c] Tuset-Peiró, P., Gomes, R. D., Thubert, P., Cuerva, E., Egusquiza, E., and Vilajosana, X. (2020c). A dataset to evaluate ieee 802.15.4g sun for dependable low-power wireless communications in industrial scenarios. *MDPI Data*, XX(XX).

[Watteyne et al., 2010] Watteyne, T., Lanzisera, S., Mehta, A., and Pister, K. S. J. (2010). Mitigating Multipath Fading through Channel Hopping in Wireless Sensor Networks. In *2010 IEEE International Conference on Communications*, pages 1–5.

[Watteyne et al., 2009] Watteyne, T., Mehta, A., and Pister, K. (2009). Reliability through frequency diversity: Why channel hopping makes sense. In *Proceedings of the 6th ACM Symposium on Performance Evaluation of Wireless Ad Hoc, Sensor, and Ubiquitous Networks*, PE-WASUN '09, page 116–123, New York, NY, USA. Association for Computing Machinery.

[Zanella et al., 2014] Zanella, A., Bui, N., Castellani, A., Vangelista, L., and Zorzi, M. (2014). Internet of things for smart cities. *IEEE Internet of Things Journal*, 1(1):22–32.

[Zubair et al., 2016] Zubair, M. A., Nain, A. K., Bandaru, J., Rajalakshmi, P., and Desai, U. B. (2016). Reconfigurable dual mode ieee 802.15.4 digital baseband receiver for diverse iot applications. In *2016 IEEE 3rd World Forum on Internet of Things (WF-IoT)*, pages 389–394.

Appendix A

Additional Tables

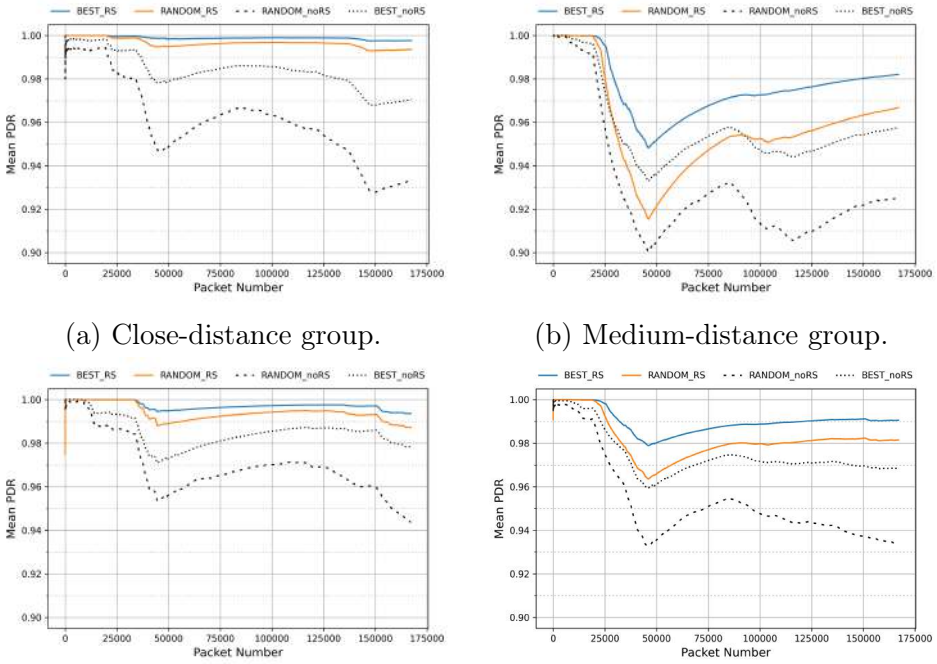

(a) Close-distance group.

(b) Medium-distance group.

(c) Far-distance group.

(d) All sensors.

Figure A.1: Evolution of PDR values for a value of 3 re-transmissions per packet for *RANDOM* and *BEST* modulation selection strategies with and without energy shaping for different nodes groups.

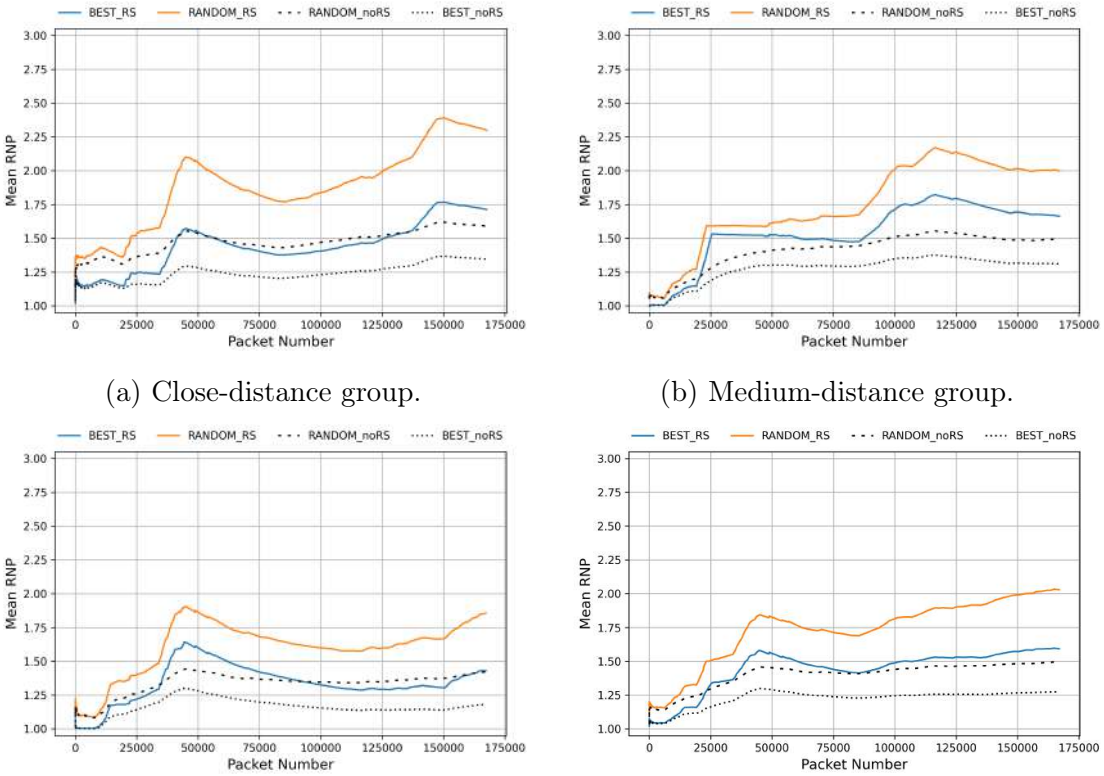

(a) Close-distance group.

(b) Medium-distance group.

(c) Far-distance group.

(d) All sensors.

Figure A.2: Evolution of RNP values for a value of 3 re-transmissions per packet for *RANDOM* and *BEST* modulation selection strategies with and without energy shaping for different nodes groups.

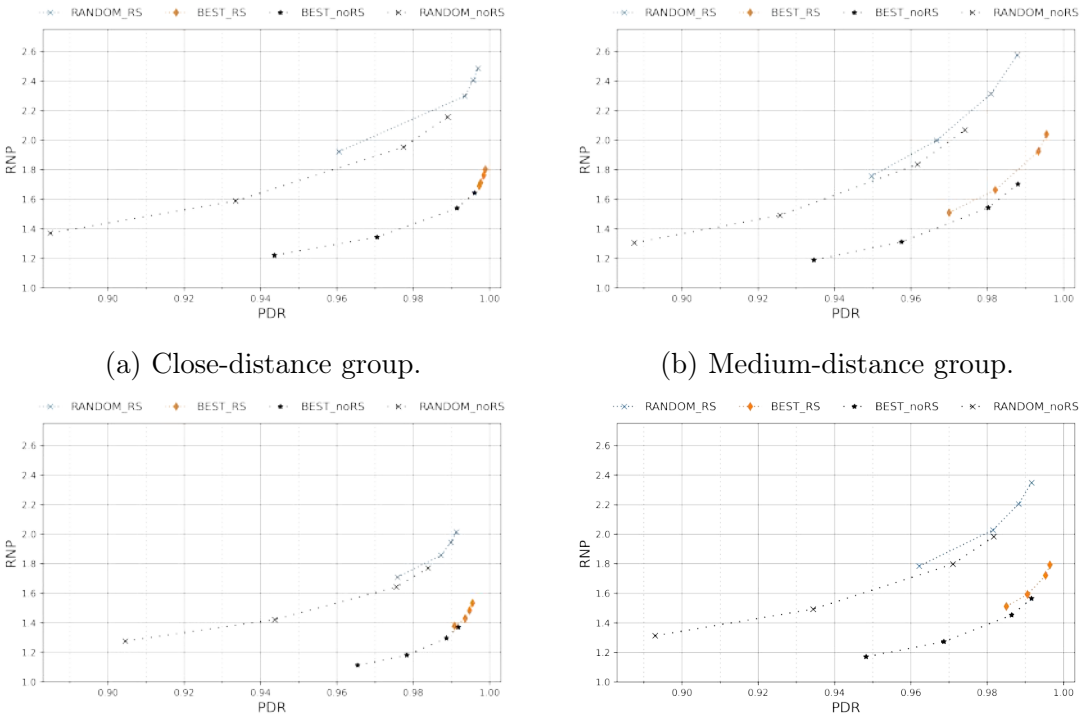

(a) Close-distance group.

(b) Medium-distance group.

(c) Far-distance group.

(d) All sensors.

Figure A.3: Final PDR-RNP values for different values of re-transmission numbers (i.e. 1, 2, 3, 6 and 9 re-transmissions per packet) for *RANDOM* and *BEST* modulation selection strategies modulation selection strategies with and without energy shaping for different nodes groups.

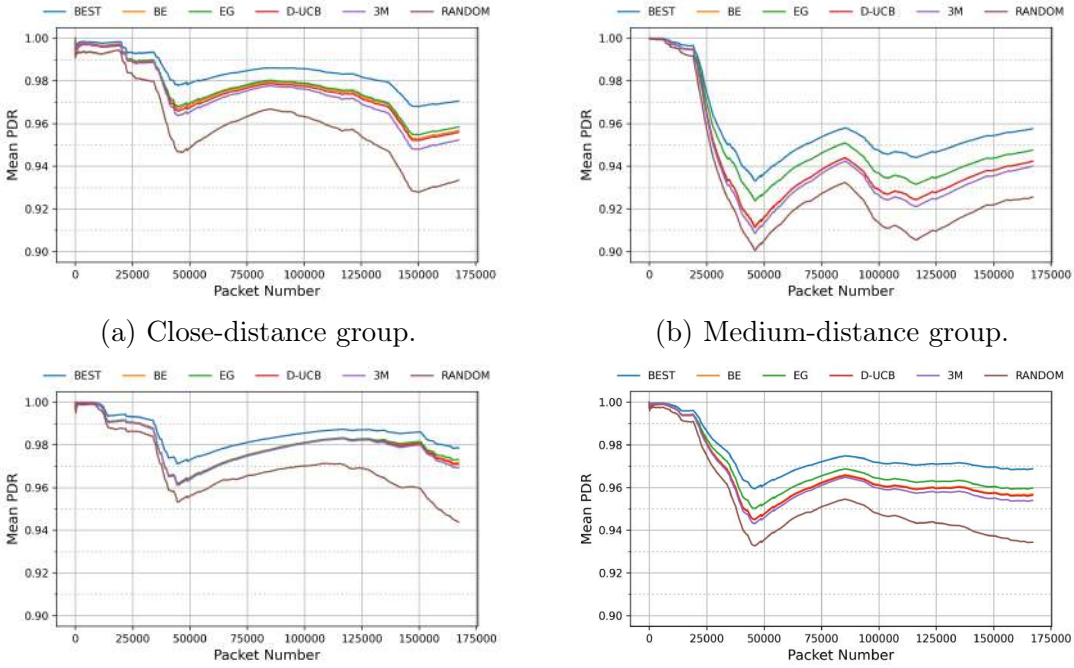

(a) Close-distance group.

(b) Medium-distance group.

(c) Far-distance group.

(d) All sensors.

Figure A.4: Evolution of PDR values for a value of 3 re-transmissions per packet for all the modulation selection strategies without energy shaping for different nodes groups.

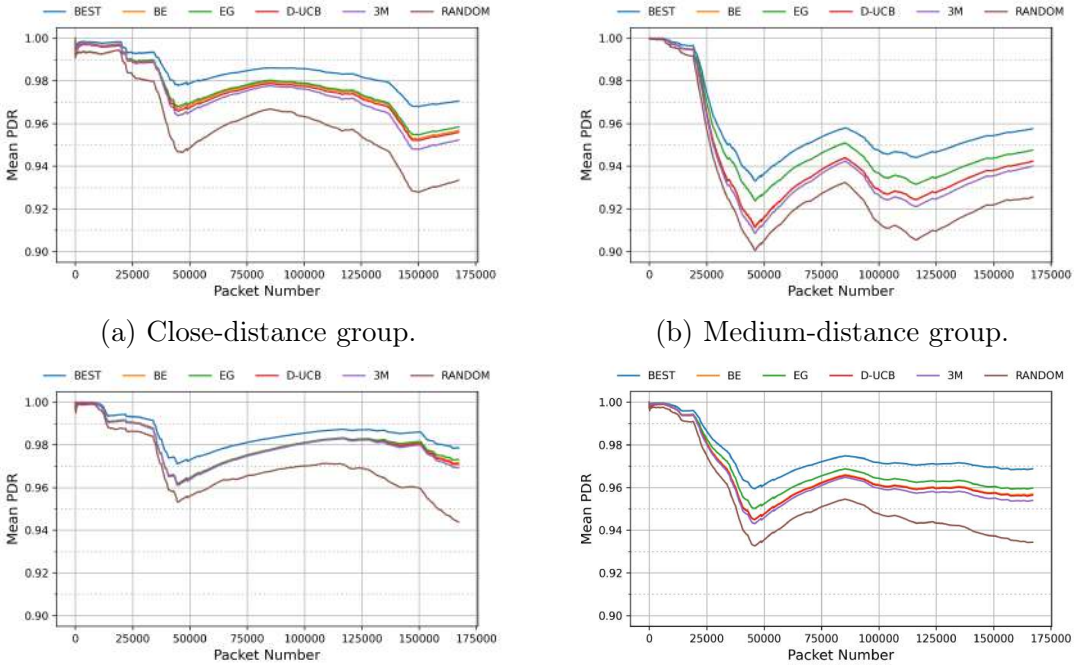

(a) Close-distance group.

(b) Medium-distance group.

(c) Far-distance group.

(d) All sensors.

Figure A.5: Evolution of PDR values for a value of 3 re-transmissions per packet for all the modulation selection strategies without energy shaping for different nodes groups.

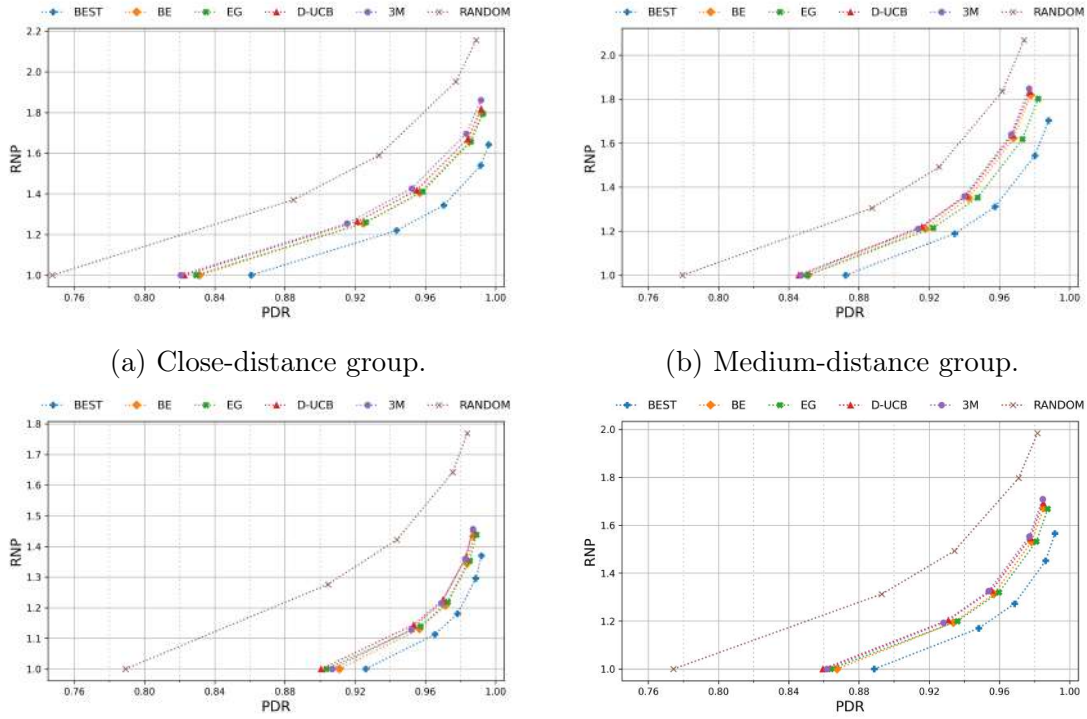

(a) Close-distance group.

(b) Medium-distance group.

(c) Far-distance group.

(d) All sensors.

Figure A.6: Final PDR-RNP values for different values of re-transmission numbers (i.e. 1, 2, 3, 6 and 9 re-transmissions per packet) for all the modulation selection strategies without energy shaping for different nodes groups.

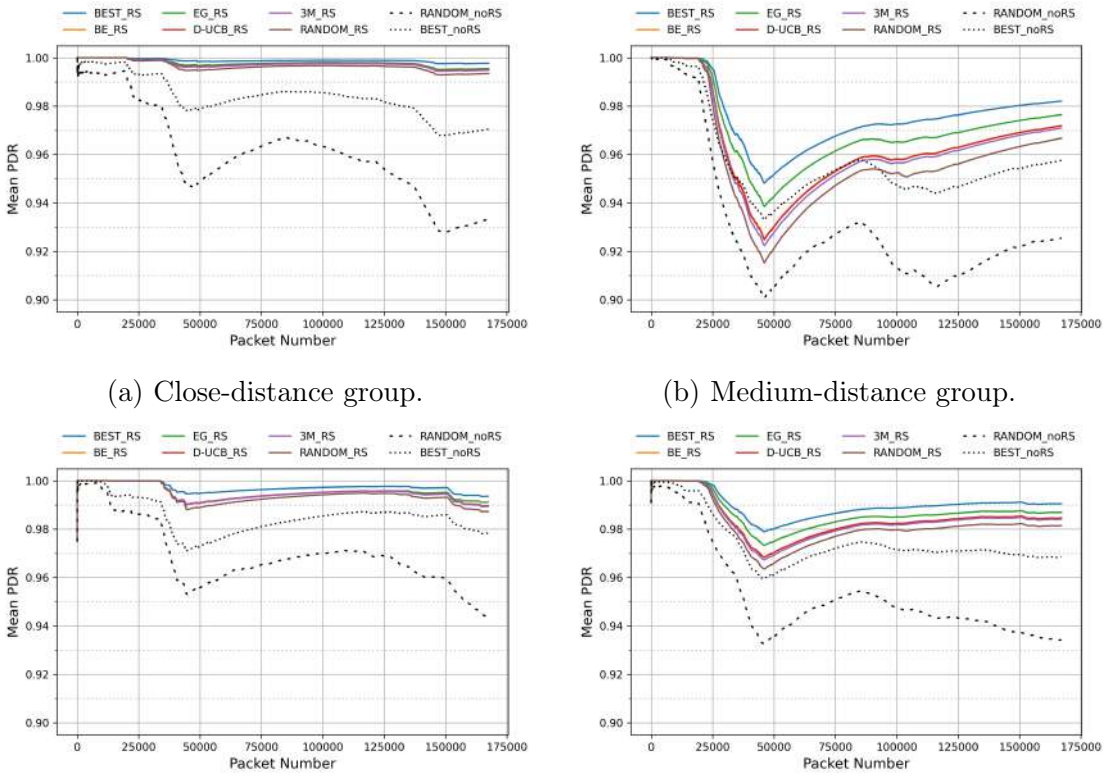

(a) Close-distance group.

(b) Medium-distance group.

(c) Far-distance group.

(d) All sensors.

Figure A.7: Evolution of PDR values for a value of 3 re-transmissions per packet for all the modulation selection strategies with energy shaping for different nodes groups. Baseline tracks for *RANDOM* and *BEST* strategies without energy shaping for the same re-transmission value are included for comparison.

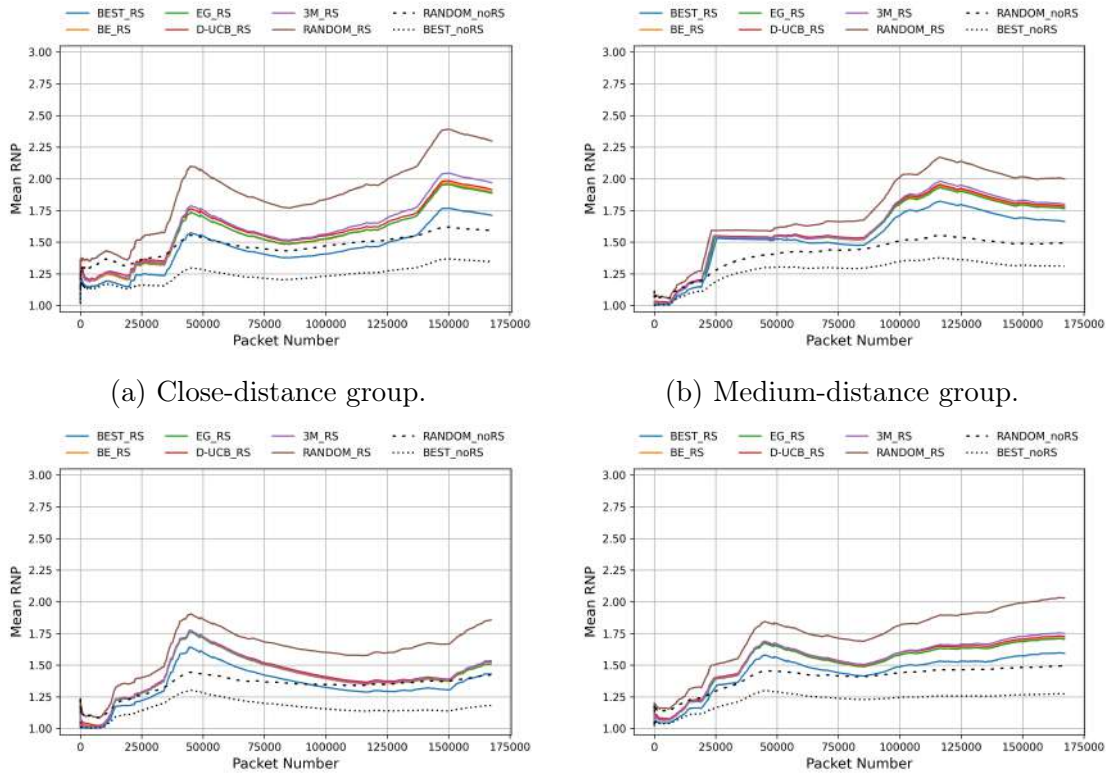

(a) Close-distance group.

(b) Medium-distance group.

(c) Far-distance group.

(d) All sensors.

Figure A.8: Evolution of RNP values for a value of 3 re-transmissions per packet for all the modulation selection strategies with energy shaping for different nodes groups. Baseline tracks for *RANDOM* and *BEST* strategies without energy shaping for the same re-transmission value are included for comparison.

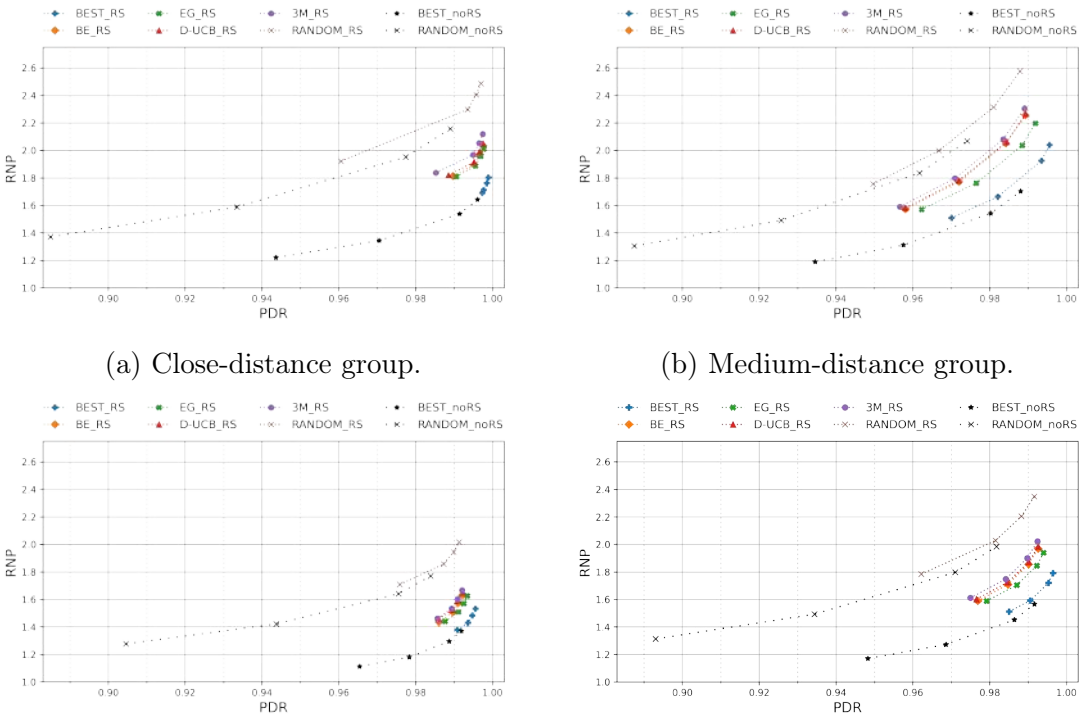

(a) Close-distance group.

(b) Medium-distance group.

(c) Far-distance group.

(d) All sensors.

Figure A.9: Final PDR-RNP values for different values of average re-transmission numbers (i.e., 2, 3, 6 and 9 re-transmissions per packet and $N_{\text{MAX\_SURPLUS}}$=9) for all the modulation selection strategies with energy shaping for different nodes groups. Baseline tracks for *RANDOM* and *BEST* strategies without energy shaping for the same set of re-transmission values are included for comparison.